

Advances on the investigation of landslides by space-borne synthetic aperture radar interferometry

Roberto Tomás, Qiming Zeng, Juan M. Lopez-Sanchez, Chaoying Zhao, Zhenhong Li, Xiaojie Liu, María I. Navarro-Hernández, Liuru Hu, Jiayin Luo, Esteban Díaz, William T. Szeibert, José Luis Pastor, Adrián Riquelme, Chen Yu & Miguel Cano

To cite this article: Roberto Tomás, Qiming Zeng, Juan M. Lopez-Sanchez, Chaoying Zhao, Zhenhong Li, Xiaojie Liu, María I. Navarro-Hernández, Liuru Hu, Jiayin Luo, Esteban Díaz, William T. Szeibert, José Luis Pastor, Adrián Riquelme, Chen Yu & Miguel Cano (07 Nov 2023): Advances on the investigation of landslides by space-borne synthetic aperture radar interferometry, Geo-spatial Information Science, DOI: [10.1080/10095020.2023.2266224](https://doi.org/10.1080/10095020.2023.2266224)

To link to this article: <https://doi.org/10.1080/10095020.2023.2266224>



© 2023 Wuhan University. Published by Informa UK Limited, trading as Taylor & Francis Group.



[View supplementary material](#)



Published online: 07 Nov 2023.



[Submit your article to this journal](#)



Article views: 66



[View related articles](#)



[View Crossmark data](#)

Advances on the investigation of landslides by space-borne synthetic aperture radar interferometry

Roberto Tomás ^a, Qiming Zeng ^b, Juan M. Lopez-Sanchez ^c, Chaoying Zhao ^d, Zhenhong Li ^d,
Xiaojie Liu ^{a,e}, María I. Navarro-Hernández ^a, Liuru Hu ^{a,f,g}, Jiayin Luo ^c, Esteban Díaz ^a,
William T. Szeibert ^h, José Luis Pastor ^a, Adrián Riquelme ^a, Chen Yu ^d and Miguel Cano ^a

^aDepartamento de Ingeniería Civil, University of Alicante, Alicante, Spain; ^bInstitute of Remote Sensing and Geographic Information System, School of Earth and Space Science, Peking University, Beijing, China; ^cInstitute for Computer Research (IUII), University of Alicante, Alicante, Spain; ^dCollege of Geological Engineering and Geomatics, Chang'an University, Xi'an, China; ^eSchool of Civil Engineering, Lanzhou University of Technology, Lanzhou, China; ^fLand Satellite Remote Sensing Application Center (LASAC), Ministry of Natural Resources of P.R. China, Beijing, China; ^gThe First Topographic Surveying Brigade of Ministry of Natural Resources of the People's Republic of China, Xi'an, China; ^hSixense, Departamento Satélite, L'Hospitalet de Llobregat, Barcelona, Spain

ABSTRACT

Landslides are destructive geohazards to people and infrastructure, resulting in hundreds of deaths and billions of dollars of damage every year. Therefore, mapping the rate of deformation of such geohazards and understanding their mechanics is of paramount importance to mitigate the resulting impacts and properly manage the associated risks. In this paper, the main outcomes relevant to the joint European Space Agency (ESA) and the Chinese Ministry of Science and Technology (MOST) Dragon-5 initiative cooperation project ID 59,339 "Earth observation for seismic hazard assessment and landslide early warning system" are reported. The primary goals of the project are to further develop advanced SAR/InSAR and optical techniques to investigate seismic hazards and risks, detect potential landslides in wide regions, and demonstrate EO-based landslide early warning system over selected landslides. This work only focuses on the landslide hazard content of the project, and thus, in order to achieve these objectives, the following tasks were developed up to now: a) a procedure for phase unwrapping errors and tropospheric delay correction; b) an improvement of a cross-platform SAR offset tracking method for the retrieval of long-term ground displacements; c) the application of polarimetric SAR interferometry (PolInSAR) to increase the number and quality of monitoring points in landslide-prone areas; d) the semiautomatic mapping and preliminary classification of active displacement areas on wide regions; e) the modeling and identification of landslides in order to identify triggering factors or predict future displacements; and f) the application of an InSAR-based landslide early warning system on a selected site. The achieved results, which mainly focus on specific sensitive regions, provide essential assets for planning present and future scientific activities devoted to identifying, mapping, characterizing, monitoring and predicting landslides, as well as for the implementation of early warning systems.

ARTICLE HISTORY

Received 9 January 2023
Accepted 28 September 2023

KEYWORDS


InSAR; SAR offset tracking;
PolInSAR; landslide;
mapping; modeling; early
warning; monitoring


1. Introduction

Landslides are destructive geohazards to people and infrastructure, resulting in hundreds of deaths and billions of dollars of damage every year (Highland and Bobrowsky 2008). In Italy alone over 480,000 landslides were recorded between 1999 and 2010 (Solari et al. 2020), and this number has now exceeded 620,000 landslides (Confuorto et al. 2023; Iadanza et al. 2021), representing the second largest cause of loss of life and damage to buildings, infrastructure, and cultural heritage, due to natural physical processes after earthquakes in that country. In the United States, it is estimated that landslides cause more than 1000 million dollars in damage each year and about 25 to 50 fatalities (USGS 2022). More recently, the

Centre for Research on the Epidemiology of Disasters (CRED) published its 2021 annual report indicating that 474 people died in 2021 in the world due to landslides, causing economic losses worth 500 million dollars (CRED 2022).

Large areas of mountain landscapes worldwide are broadly susceptible to landslides, which often occur suddenly, prompting rapid and destructive runoff downslope. Landslides are also a major secondary hazard in most continental earthquakes, including the 1999 Chi-Chi (Lin et al. 2007), 2005 Kashmir (Owen et al. 2008), 2008 Wenchuan (Yin, Wang, and Sun 2009), and 2015 Gorkha (Lacroix 2016) events. Their consequences can be devastating; over 32,000 deaths from the more than 200,000 deaths in the 1920

CONTACT Roberto Tomás  roberto.tomas@ua.es

 Supplemental data for this article can be accessed online at <https://doi.org/10.1080/10095020.2023.2266224>.

© 2023 Wuhan University. Published by Informa UK Limited, trading as Taylor & Francis Group.

This is an Open Access article distributed under the terms of the Creative Commons Attribution License (<http://creativecommons.org/licenses/by/4.0/>), which permits unrestricted use, distribution, and reproduction in any medium, provided the original work is properly cited. The terms on which this article has been published allow the posting of the Accepted Manuscript in a repository by the author(s) or with their consent.

Haiyuan earthquake may have been caused by landslides (Xu et al. 2021).

Landslides also extend far from areas affected by surface rupture and have deleterious long-term effects on the landscape, leading to widespread aggradation and flooding, and causing increased sediment loads that are likely to persist for decades (Koi et al. 2008). Recent catastrophic landslides have demonstrated the importance of understanding this hazard and of developing early-warning systems. Therefore, the early detection of landslides, the automatic mapping and monitoring of the rate of deformation of such geohazards, and understanding their mechanics and causative factors are of paramount importance to mitigate the resulting impacts and properly manage the associated risks.

Furthermore, developing and validating technology for direct monitoring of landslide hazards meets the Sentinel-1 mission objective of geological mapping (Geudtner et al. 2014; Torres, Snoeij, Geudtner, et al. 2012; Torres, Snoeij, Davidson, et al. 2012). The capability of Interferometric SAR (InSAR) to identify, map and monitor landslides over wide areas has been demonstrated over the past 30 years. In April 2014, Sentinel-1A was launched, and has been collecting data routinely over more than 5 years. Sentinel-1B was launched in 2016. Moreover, in 2018, the Spanish X-band satellite PAZ (“peace” in Spanish) was launched, increasing the number of operative satellites which could be used for monitoring landslides.

Therefore, earth observation techniques, and in particular InSAR, have become a unique technology which has revolutionized our capability to measure ground surface displacements globally and with extraordinary resolution for a large number of applications and uses in the field of geohazards (Biggs and Wright 2020; Tomás and Li 2017), and more specifically in the field of landslides (Jia et al. 2022; Tzouvaras, Danezis, and Hadjimitsis 2020b; Yao, Yao, and Liu 2022; Zhao and Lu 2018). Some papers highlight the usefulness of InSAR technologies for the study of landslides (e.g. Colesanti and Wasowski 2006; Mondini et al. 2021; Solari et al. 2020).

To analyze the trends, patterns, and major milestones in the field of InSAR techniques for monitoring landslides over time, we conducted a bibliometric study using the Web of Science (WoS) website. By presenting the trends and patterns found in publications related to landslides and InSAR, we highlight the importance and current relevance of our research, thereby enhancing its impact. Additionally, the inclusion of the bibliometric analysis serves the purpose of offering a contextual backdrop for our study. It enables readers to comprehend the research evolution in this domain and acknowledge the advancements achieved over time. To achieve this analysis, some specific data collection criteria were defined to obtain

a more accurate information retrieval. The terms related to the earth observation technique (i.e. “InSAR” or “DInSAR” or “PSInSAR” or “PS-InSAR” or “SAR interferometry” or “persistent scatterers”) and the geological process to be measured (i.e. “landslide*” or “landslip*” or “mass movement*”) were used to search for specific papers of interest. These two groups of terms were combined by means of the Boolean operator “AND” in order to get all the contributions related to the measured process and the measuring technique. It should be noted that the asterisk (*) includes any group of characters and even no characters (e.g. landslide* includes landslide and landslides) and quotation marks (“) search for exact phrases for compound terms (e.g. persistent scatterers).

Figure 1 shows the total number of results as well as the results restricted to the “Remote sensing” and “Geotechnical engineering” meso-level citation topics from 1995 to 2022. As can be seen in the figure, the first papers showing the application of InSAR to study landslides were published in 1995 (Fruneau, Achache, and Delacourt 1996), 2 years after the first practical demonstration of InSAR to measure the surface deformations caused by the Landers earthquake in California in 1992 (Massonnet et al. 1993). Since then, there has been a progressive increase in yearly publications about InSAR and landslides (including all the equivalent terms described above), partially motivated by important milestones in the field of InSAR, as the development of persistent scatterer interferometry (Ferretti, Prati, and Rocca 2000) or the recent launch of Sentinel satellites, among others (Figure 1).

The analyzed datasets provide a very good fit to a power model with a high coefficient of determination (0.903 and 0.910 for “Remote sensing” and “Geotechnical engineering” meso-level citation topics, respectively) in agreement with the conclusions achieved by Gupta and Karisiddappa (2000) for a different scientific literature. This growth is more than double in the field of “Remote sensing” than “Geotechnical engineering”. It should be noted that most of the contributions published in the field of “Remote sensing” are mostly focused on topics related to improvements in the processing for landslide detection and monitoring. In contrast, the papers published in the field of “Geotechnical engineering” are more focused on the geotechnical process, using InSAR as a tool for the study of landslides.

Consequently, based on this simple bibliometric analysis we can conclude that: a) although InSAR was born last century, it is still a growing topical issue which enables a wide variety of applications for the study of landslides and shows a great deal of maturity in this field (i.e. almost 30 years); (b) the capability of InSAR to study landslides has been demonstrated, and, as a consequence, InSAR has

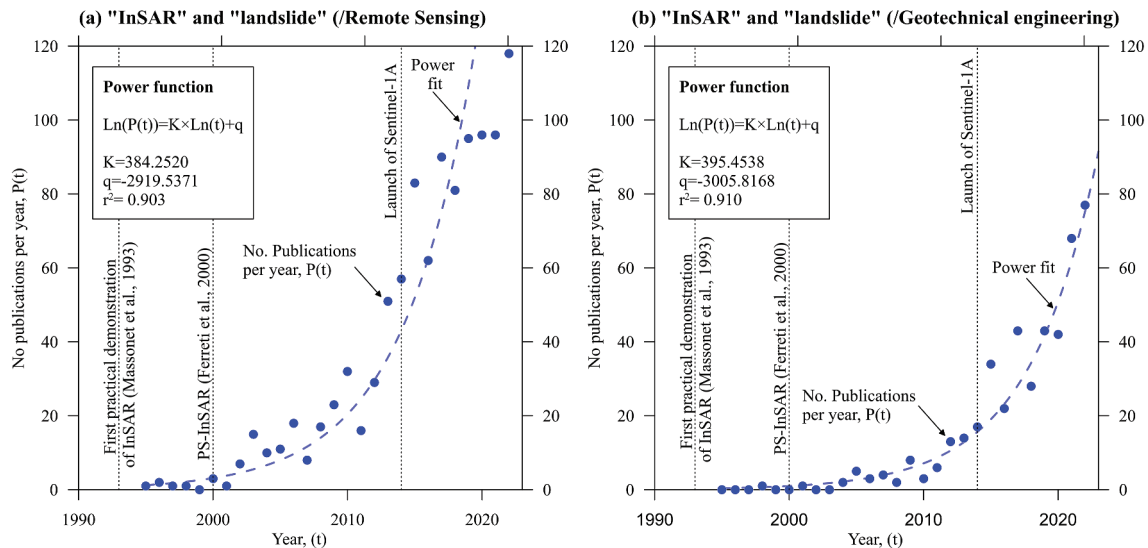


Figure 1. Growth of the number of yearly publications (dots) in the database Web of Science (WoS) containing the terms “InSAR” and “landslide” (including all the equivalent terms described in the text) in the meso-level citation topics (a) “Remote sensing” and (b) “Geotechnical engineering” between 1995 and 2022. Note that the searches are restricted to (a) “Remote sensing”; and (b) Geology segments in the Web of Science. The dashed lines represent the best fit power function of the dots. Some key milestones in the field of InSAR have been plotted as vertical dotted lines.

become consolidated on the field of geotechnics as a tool for the study of landslides; and (c) according to the trend observed in the field of “Geotechnical engineering”, an increase in the number of practical applications of InSAR for the study of landslides is expected in the upcoming years. Undoubtedly, all these aspects highlight the relevance of the topic addressed in this article and the importance of continuing to advance in the application of InSAR techniques in the field of landslides.

This paper presents the midterm results achieved within the framework of the joint European Space Agency (ESA) and the Chinese Ministry of Science and Technology (MOST) Dragon-5 initiative cooperation project titled “Earth observation for seismic hazard assessment and landslide early warning system” (reference Dragon 5 ID 59,339). More details about the project can be found on the Dragon 5 Cooperation Programme webpage (<https://dragon5.esa.int/projects/earth-observation-for-seismic-hazard-assessment-and-landslide-early-warning-system/>).

The study focuses on five landslide-prone study areas located in China (Deqin county, Wudongde reservoir, and Jinsha River) and Spain (Alcoy, and La Unión). SAR interferometry techniques were utilized within the Dragon 5 project (ID 59,339), as shown in Figure 1, to investigate and analyze these areas. It is crucial to note that all of these study areas share a common characteristic: they exhibit a high susceptibility to landslides, posing a potential threat to infrastructure and human safety due to their destructive nature.

To advance the investigation of landslides using space-borne SAR interferometry, this work highlights

the importance of developing new processing procedures to enhance InSAR accuracy. It also emphasizes the utilization of improved SAR offset tracking and Polarimetric SAR interferometry methods for monitoring purposes. Moreover, the proposal of automated procedures to map landslides in large-scale regional areas using InSAR datasets, the development of various InSAR-supported landslide modeling approaches, and the utilization of InSAR data for early landslide warning systems are considered essential components.

The obtained results bring significant advancements concerning the exploitation of InSAR data for landslide identification, monitoring, and early warning, resulting in a deeper understanding of the triggering factors involved in the slope stability processes.

2. Description of the study area

Five areas, three in China (i.e. Deqin county, the Shandong landslide, and the Laojingbian landslide) and two in Spain (i.e. the mining area of La Unión, and the valley of Alcoy), have been subject of study during the first 2 years of this DRAGON project (Figure 2). All of them share a common characteristic: their high susceptibility to landslides and that they pose a major threat to infrastructure and human safety. In the following paragraphs, all these study zones are briefly described.

Alcoy is an important industrial city placed on a fluvial valley of the SE of Spain (Figure 2) prone to landslides Delgado et al. (2004). It belongs to the Prebetic Unit of the External Zone of the Betic cordillera and develops on a Neogene-Quaternary basin

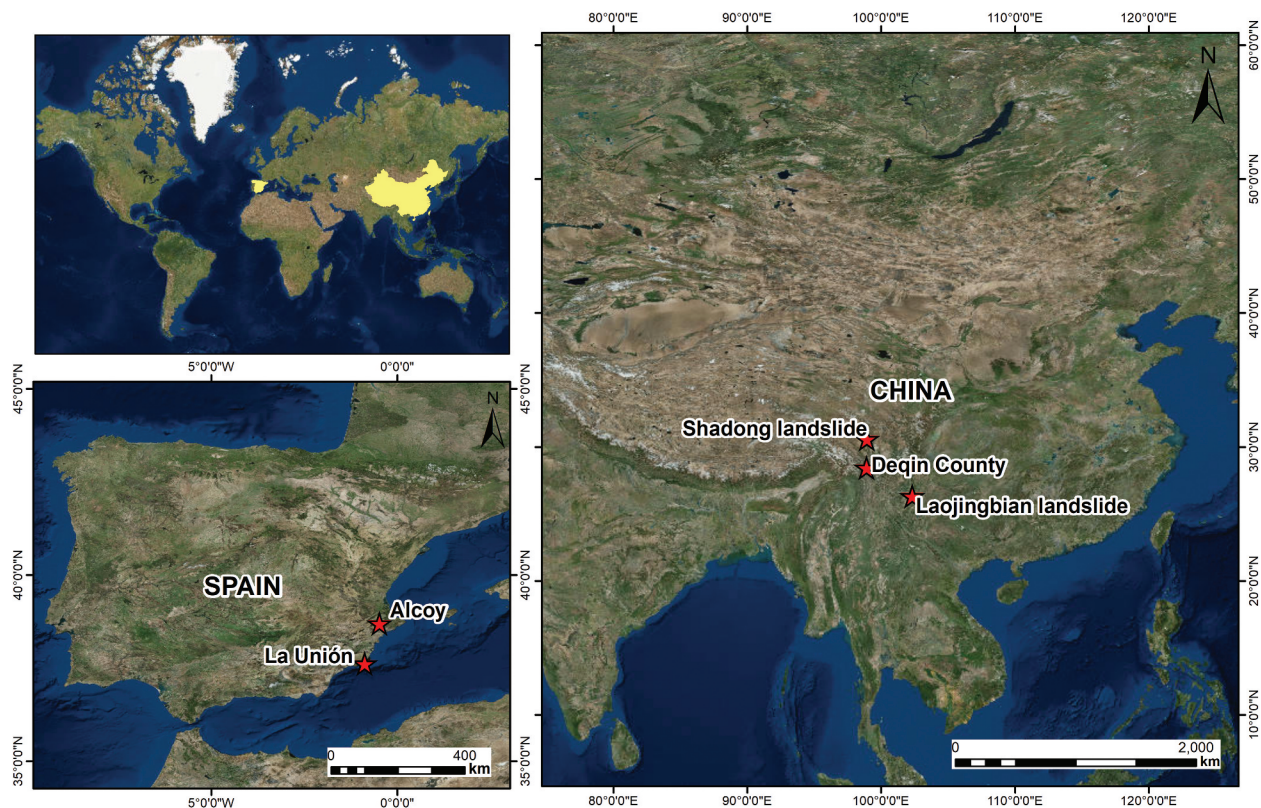


Figure 2. Location of the study zones.

(Almela et al. 1975). Landslides mainly develop on Neogene marine marls (named Tap formation) that can reach up to 400 m thickness (IGME 1985a) in some points of the valley. The combination of a steep relief, poor geotechnical properties of the soil units, torrential rainfalls, and a moderate seismic activity make this area highly susceptible to landslides (Delgado et al. 2004, 2006; IGME 1985a).

Deqin County is placed in the southern border of the Tibetan Plateau (SW China) (Figure 2). Its geology is very complex due to the existing compressive tectonics leading to important large faults and a steep relief with elevations varying from 1924 to 6740 m a.s.l. The study area presents a cold temperate mountain monsoon climate and a high seismicity, being rainfall and earthquakes, jointly with anthropogenic activities, the main triggering factors of landslides. Falls, slides and flows are widely distributed in Deqin County, affecting multiple infrastructure and urban areas.

The Shadong landslide is a giant translational slide according to Cruden and Varnes (1996), with an approximate extension of 5.33 km², placed on the right bank of the Jinsha River, in Gongjue County, Tibet, China (Figure 2). As a result of the quick uplift of the Qinghai-Tibet Plateau, this area presents a strong orography with maximum heights of 4000 m a.s.l. and differences in elevation between 500 and 2000 m (Li, Fan, and Cheng 2006; Wang et al. 2000). The Jinsha River, which runs the area, has created deep V-shaped valleys. The study zone presents

a continental plateau monsoon, registering a mean accumulated rainfall of 480 mm, mainly concentrated during the summer, and an annual average temperature of 6.5 °C. These meteorological conditions exert a strong effect on rocks leading to a very strong weathering. Tectonically, the area is affected by a series of NW-oriented active faults that present an important seismic activity (Chen et al. 2013). Therefore, geological, climatic and topographic conditions, jointly with the seismic activity, the rainfall patterns and the action of the river, induce large-scale pull-type landslides such as Shadong landslide.

The Laojingbian landslide (Figure 2) has also been the subject of research in this project. This landslide is placed in the Wudongde reservoir area, located in the lower reaches of the Jinsha River in Yunnan Province (China). Regarding the area's geology, it is placed on a tectonically active southeast edge of the Qinghai-Tibet Plateau, characterized by the existence of deep and narrow valleys and high reliefs (Wang et al. 2013; Zhao et al. 2018). This area presents a subtropical monsoon climate with annual accumulated precipitations up to 800 mm, mainly concentrated from June to October, and huge daily temperature variations that play an important role on the weathering of the rocks and soils that constitute the slopes (Zhao et al. 2018). The combination of heavy rainfalls and seismic activity jointly with the important weathering action makes this area very prone to landslides under natural conditions. Moreover, the Wudongde reservoir

management activities cause important periodic water-level changes in the river, strongly affecting the stability of the margins of the river (Wang et al. 2013).

The mining area of La Unión is placed on the SE coast of Spain (Figure 2). It is a metal mining (Pb and Zn ore deposits) area located in the Internal Zones of the Betic Cordillera that was exploited from the Roman times up to 1991 (Herrera et al. 2007). The abandoned open-pit mines and the tailing dumps present a deficient stability exhibiting multiple large slope instabilities (López-Vinielles et al. 2021). These instabilities are mainly induced by intense rainfall periods that usually occur during the autumn. Additionally, the large waste dumps are under a gradual process of consolidation. Therefore, these processes pose a threat to the surrounding urban areas and constitute an important obstacle for the economic and environmental recuperation of this mining area (Herrera et al. 2007).

3. Materials and methods

Figure 3 provides a schematic summary of the various applications resulting from the project and the study areas in China and Spain where they have been implemented. As can be observed, this methodological section and the subsequent results section of the paper have been divided into six distinct subsections, each addressing different applications. This subdivision aims to enhance the readability of the paper. However, the Earth Observation (EO) data, auxiliary datasets, and field campaigns conducted for each study area, along with their respective sources of information and the utilization of each dataset, are summarized in Table 1. It should also be noted that a validation process of InSAR

datasets has been conducted for the five study cases (refer to supplementary material S1). Validation is crucial to evaluate the precision and dependability of the derived measurements. Through the comparison of InSAR results with ground truth information, such as ancillary inventories or geo-information, as well as independent in situ measurements, like GNSS data or other monitoring data, the validation process ensures the completeness, consistency, and accuracy of the InSAR datasets used in this work.

3.1. Procedure for phase-unwrapping errors and tropospheric delay correction

In the deformation monitoring of landslides in areas with complex geomorphological and environmental conditions (e.g. humid climate, dense vegetation and steep terrain), the InSAR interferograms are usually biased by wrong integer number of cycles (2π rad) added to the interferometric phase during the two-dimensional phase unwrapping, to which we refer simply to as unwrapping errors (Kovács et al. 2019; Tzouvaras, Danezis, and Hadjimitsis 2020a; Wasowski and Bovenga 2014). In the Dragon project, we have developed an approach that combines information from both the spatial and temporal domains to efficiently correct the unwrapping errors in a network of interferograms. The method is composed of two procedures. We first correct the obvious phase unwrapping errors in each interferogram using information from the spatial domain. For this purpose, the areas with obvious phase unwrapping errors in each interferogram are first determined, and then the corrected unwrapping phase is obtained by adding or subtracting an integer number of phase cycle(s) (i.e. phase ambiguity) to pixels contaminated with unwrapping errors. In the temporal domain, we use the principle of

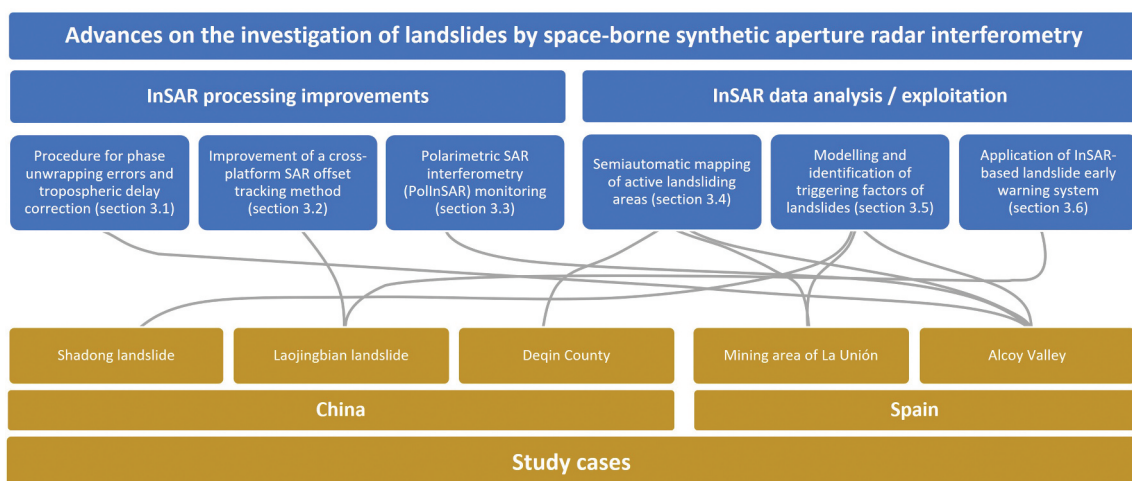


Figure 3. Scheme depicting the contributions of this study and the test areas in which they have been implemented.

Table 1. Summary of the datasets used in the different study areas.

Study area	Data collection/campaign/dates	Resolution/scale/frequency	Source	Use
Valley of Alcoy, Alicante Province, Spain	21 PAZ asc. Images (09/09/2019–07/02/2021)	0.87 × 0.45 m	National Institute of Aerospace Technology (INTA)	Processing
	186 Sentinel-1 asc. Images (02/01/2007–28/02/2011)	2.33 × 13.98 m	ESA	Processing
	Permanent GNSS station (01/09/2019–01/12/2020)	Does not apply	Instituto Cartográfico Valenciano (ICV)	Validation
	Surveying (01/12/2019–01/05/2020)	Sparse points	Ministerio de Fomento	Validation
	Damage assessment (November 2021)	Does not apply	Own field campaign	Validation
	Geomorphological map (November 2021)	1:2000	Geological survey of Spain (IGME)	Characterization/validation
	Landslide inventory map (created in 1985)	1:5000	Spanish Meteorological Agency (AEMET)	Validation
	Rainfall time series (09/09/2019–07/02/2021)	Daily	Geological survey of Spain (IGME)	Triggering factors analysis
	Geological map (created in 1975)	1:50000	Geological survey of Spain (IGME)	Conditioning factor analysis
	Geotechnical data (from a report published in 1985)	Does not apply	National Geographic Institute (IGN)	Modelling
	Seismic catalog (2019–2021)	Does not apply	National Center for Geographic Information (CNIG)	Triggering factors analysis
	Digital surface model (created in 2016)	5 × 5 m	National Center for Geographic Information (CNIG) and Ministerio de Fomento	Processing
	Technical report about specific landslides (from 1985 to 2011)	Does not apply	Geological survey of Spain (IGME)	Validation
106 Sentinel-1 asc. Images (11/04/2017–08/05/2021)	2.33 × 13.98 m	ESA	Processing	
117 Sentinel-1 des. Images (25/03/2017–08/06/2021)	2.33 × 13.98 m	ESA	Processing	
Landslide inventory map (18/09/2020)	~1:1000 (derived from UAV)	China Institute of Geo-environment Monitoring	Validation	
Optical satellite images (2017–2021)	0.6 × 0.6 m	National Platform for Common Geospatial Information Services	Photointerpretation	
UAV optical images (18/09/2020)	0.1 × 0.1 m	Own field campaign	Photointerpretation	
Digital surface model (Created in 2013)	30 × 30 m	NGA-NASA	Processing	
16 ALOS/PALSAR-1 asc. Images (02/01/2007–28/02/2011)	4.68 × 3.17 m	JAXA	Processing	
17 ENVISAT ASAR des. Images (21/02/2007–13/10/2010)	7.80 × 4.04 m	ESA	Processing	
79 Sentinel-1 asc. Images (12/10/2014–03/10/2018)	2.33 × 13.98 m	ESA	Processing	
53 Sentinel-1 des. Images (01/12/2016–03/11/2018)	2.33 × 13.98 m	ESA	Processing	
Digital surface model (Created in 2013)	30 × 30 m	NGA-NASA	Processing	
Geomorphological map (created in 2020)	~1:1000 (derived from UAV)	Own field campaign	Characterization/validation	
14 ALOS/PALSAR-1 asc. images (27/08/2007–07/03/2011)	4.29 × 3.78 m	JAXA	Processing	
12 ALOS/PALSAR-2 asc. Images (26/09/2014–15/05/2020)	4.29 × 3.78 m	JAXA	Processing	
Seismic catalog (2007–2019)	Does not apply	China Earthquake Network Center (CENC)	Triggering factors analysis	
Digital surface model (Created in 2013)	30 × 30 m	NGA-NASA	Processing	
131 Sentinel-1 asc. images (7/10/2016–10/11/2021)	2.33 × 13.98 m	ESA	Processing	
131 Sentinel-1 des. images (7/10/2016–10/11/2021)	2.33 × 13.98 m	ESA	Processing	
Landslides' inventory map (created in 1996 and updated in 2010)	~1:5000	Geological survey of Spain (IGME)	Validation	
LIDAR point clouds (2009 and 2016)	0.5 points/m ²	National Centre for Geographic Information (CNIG)	Change detection	
Geological map (created in 2008)	~1:5000	Geological survey of Spain (IGME)	Conditioning factor analysis	
Geotechnical data (from a report published in 1996)	Does not apply	Geological survey of Spain (IGME)	Modelling	
Digital surface model (created in 2016)	5 × 5 m	National Center for Geographic Information (CNIG)	Processing	

the consistency of triplets of interferometric phases to correct phase unwrapping errors (Yunjun, Fattahi, and Amelung 2019).

Atmospheric delays within individual interferograms can be in the range of tens of centimeters (Murray, Lohman, and Bekaert 2021), thus potentially masking small-gradient ground displacements. To address this issue, in the Dragon project, we proposed a block-based correction approach for atmospheric delays. It comprises four main steps: Principal Component Analysis (PCA) decomposition, masking of active displacement areas, estimation and correction of atmospheric delays, and estimation of corrected displacement rate and time series. First, the PCA is applied to separate the displacement signals and the atmospheric delays. Second, the active displacement areas are determined using the decomposed results. Then, in order to avoid any estimation bias in the atmospheric delays caused by displacement signals, all the active displacement areas are masked out from the unwrapped interferograms. Next, the atmospheric delays are estimated based on the masked interferograms. This consists of two stages: we first divided the whole interferogram into several blocks considering the spatial variability of tropospheric properties, and then the atmospheric delays in each block are computed with a quadratic model. Finally, the accurate displacement rate and time series are re-estimated using the corrected unwrapped interferogram stack.

3.2. Improvement of a cross-platform SAR offset tracking method for the retrieval of ground displacements

In order to estimate the long-term time-series displacement of landslides over 10 years, we developed an improved cross-platform SAR offset-tracking method (Liu et al. 2020; Yin et al. 2022). The new approach enables the estimation of the two-dimensional offsets between SAR images not only from an identical platform (e.g. ALOS-1 and ALOS-1) but also from cross platforms (e.g. ALOS-1 and ALOS-2).

First, for SAR images acquired from the same platform (i.e. ALOS-1 or ALOS-2), the reference images were determined based on considerations such as spatio-temporal baselines and Doppler central frequency variations. To link the SAR images from cross platforms, the reference image from the second SAR platform is set arbitrarily as the final reference image.

Secondly, all the secondary images were ortho-rectified and co-registered with respect to their corresponding reference image. The principles and steps involved in SAR ortho-rectification and co-

registration are described as follows (Li et al. 2014; Lu and Dzurisin 2010; Werner et al. 2000):

- (i) Based on the SAR imaging geometry and the external DEM (please refer to Table 1 for the datasets used in this study), the initial transformation relationship that maps the pixel locations in the primary image to their corresponding positions in the secondary image is established.
- (ii) The established transformation relationship is refined through the resampling of the reference SAR intensity image to match the geometry of the secondary intensity image. The obtained offsets between the two images are then estimated and utilized to enhance the initial transformation relationship.
- (iii) The rectified SAR images are obtained by resampling all secondary SAR images to the frame of the primary images using the refined transformation relationship.

Finally, 2-D deformation results of each offset pair were geocoded into the WGS 84 coordinate system and combined to invert 2-D deformation rate and time series using singular value decomposition.

3.3. Polarimetric SAR interferometry (PolInSAR) monitoring of active displacement areas on wide regions

Sentinel-1 (S1) images include two polarimetric channels. Most works in monitoring displacements of the Earth's surface only use the VV channel. The VH channel is discarded for its lower amplitude. Thanks to the development of Polarimetric Persistent Scatterer Interferometry (PolPSI) methods, we are aimed to integrate multi-polarization channels into a single optimal (OPT) one. The obtained OPT channel can be used in practical applications including deformation monitoring.

To this aim, for each pixel in S1 images, a vector k is defined as:

$$k = [S^{VV}, S^{VH}]^T \quad (1)$$

where S^{VV} is the vertical copolar channel, S^{VH} is the crosspolar channel, T is the transpose operator. With complex weight vector ω , PolPSI methods can project each vector k into a new scalar μ (OPT channel)

$$\mu = \omega^{*T} k \quad (2)$$

in which $*$ represents the conjugate operator. Searching for the optimum parameters in ω to minimize the selection criterion D_A , which is calculated for the whole stack of single look images. The detailed

definition of ω and searching method are introduced in Luo et al. (2022).

$$D_A = \frac{\sigma_a}{\bar{a}} = \frac{1}{|\omega^{*T}k|\sqrt{N-1}} \sqrt{\sum_{i=1}^N \left(|\omega^{*T}k_i| - \overline{|\omega^{*T}k|} \right)^2} \quad (3)$$

where σ_a and \bar{a} are the standard deviation and the mean value of the image amplitude, respectively. Overline represents the empirical mean value. N is the number of images in the time series. Points with D_A lower than an established threshold (0.25) will be selected as Persistent Scatterer Candidates (PSC).

In this study, we employed the PSI processing method Coherent Pixel Technique (CPT) for getting deformation result over these PSC. A total of 186 Sentinel-1 ascending images obtained between January 2017 and January 2021 were processed. Subsequently, a total of 4348 interferograms were obtained using two sets of thresholds for spatial and temporal baselines. The first set includes interferograms with a short temporal baseline (less than 40 days) and long perpendicular baseline (up to 400 m). The second set includes interferograms with a long temporal baseline (up to 365 days) and short perpendicular baseline (less than 50 m). These two sets provide sufficient sensitivity to DEM error and deformation rate, respectively, while avoiding excessive decorrelation. However, it should be noted that the proposed methodology is not reliant on the thresholds used to select the interferograms, as it is entirely general. Consequently, comparable deformation results could be obtained with alternative sets of interferograms. Following the steps of CPT, the selected PSCs are linked by a Delaunay triangulation. The phase increment between two neighboring PSCs at one interferogram is expressed as a function of the increments of linear velocity Δv_{linear} and DEM error $\Delta \epsilon$.

More details about this methodology can be consulted in Luo et al. (2022).

3.4. Semiautomatic mapping of active landsliding areas on wide regions

The spatiotemporal delineation of potential landslide occurrences and their magnitude are important for landslide adaptation and mitigation strategies (Knevels et al. 2020). An Active Deformation Area (ADA) finder tool, called *ADA finder*, was developed by Tomás et al. (2019) and Navarro et al. (2018, 2019). This tool utilizes the methodology proposed by Barra et al. (2017) to automatically identify and map ADAs, i.e. groups of persistent scatterers which exhibit displacements, from large InSAR datasets. In brief, the methodology selects as candidates those points that

exhibit a velocity higher than a user-defined threshold usually set as twice the standard deviation of the mean velocity (σ). Then, the active points are grouped into the same ADA when their respective distances are shorter than the clustering radio, usually defined as the double of the spatial resolution.

In this Dragon project, the code has been slightly modified in Matlab software in order to increase the efficiency of the processing in wide areas in which a high number of PS is available, which is mainly suitable for high-resolution (e.g. PAZ) and wide Sentinel-1 datasets containing a high number of PS. Additionally, a new C-Index and the original “Quality Index” (QI) defined by Barra et al. (2017) were incorporated into the identification process to remove those active areas affected by important SAR geometrical distortions, residual atmospheric artifacts or phase unwrapping errors. The C-index is calculated using an external DEM (for more details, please refer to Table 1) and the image acquisition parameter geometry as:

$$\begin{aligned} C - index = & -\sin\theta \cdot \cos\alpha \cdot \cos\beta \\ & + \sin\theta \cdot \sin\alpha \cdot \cos\delta \cdot \cos\beta \\ & - \cos\theta \cdot \sin\beta \end{aligned} \quad (4)$$

where θ is the incidence angle, α is the flight direction, δ is the slope azimuth and β is the slope angle.

The line-of-sight (LOS) displacements of a pixel of a landslide derived from InSAR must present the same sign (i.e. positive or negative) as the C-index. If this condition is not met, then, the pixel can be affected by important SAR geometrical distortions and then, it is removed.

Complementarily, QI is used to evaluate the level of noise and the consistency of the standard deviation of the persistent scatterers of each ADA, providing a measurement of the degree of reliability of each detected ADA. QI = 1 and QI = 4 represent ADAs with very high and very good-quality time series, respectively. For more details about this parameter, we recommend the reading of the work published by Barra et al. (2017).

The use of the QI index or the combination of the QI index and the C-index enables us to classify the reliability of the ADAs to improve the interpretation of wide InSAR datasets.

In the DRAGON project, the original version of ADAfinder has been employed in La Unión, while the improved version was used in Deqin.

3.5. Modelling and identification of triggering factors of landslides

Landslide modeling enables us to better understand the processes and mechanisms governing landslide failures, to identify landslide triggers and conditioning factors, to evaluate the long-term slope behavior, and

to contribute in early-warning and threshold identification.

In this project, different landslide modeling tasks have been developed. In the mining area of La Unión (Murcia), a simple deterministic infinite slope geotechnical model (Skempton 1957) was applied to identify those areas in which the safety factor was lower than one (i.e. unstable) considering different hydraulic conditions of the slope through the pore pressure ratio (r_u) to consider the effect of the saturation of the slope caused by rainfall. The formula used for the calculation of the spatial distribution of the Safety Factor (SF) of the slope was adapted from the one proposed by Escobar-Wolf et al. (2021):

$$SF = \frac{c + (\gamma_m \cdot D + (\gamma_{sat} - \gamma_w - \gamma_m) \cdot H_w \cdot D) \cdot \cos^2 \beta \cdot \tan \phi}{(\gamma_m \cdot D + (\gamma_{sat} - \gamma_w - \gamma_m) \cdot H_w \cdot D) \cdot \sin \beta \cdot \cos \beta} \quad (5)$$

where c is the cohesion of the soil, γ_m and γ_{sat} are the moist (above the phreatic surface) and saturated (under the phreatic surface) unit weights of the soil, respectively, γ_w is the unit weight of the water, D is the depth of the failure surface, H_w is the height of the phreatic surface (wt) above the failure surface, normalized relatively to D , and β is the terrain slope. The obtained safety factor maps were used as ancillary information for the preliminary classification of the active deformation areas mapped from InSAR data, considering that those active areas delineated by means of InSAR datasets caused by a landslide would exhibit low slope safety factors.

In Alcoy, a slow-moving landslide affecting an important road and some protected industrial buildings from the fifteenth century cataloged as Places of Cultural Interest was analyzed using a geotechnical 3D limit equilibrium probabilistic (i.e. stochastic) and deterministic models using the software Rocscience's Slide3 2021 (Rocscience 2021). The geotechnical properties of the soil were obtained from IGME (1985b). Due to the lack of hydrological information about the slope, the effect of rainfall on the stability of the slope was evaluated considering different conditions of saturation also using the pore pressure ratio (r_u). The effect of an embankment built on the head of the landslide was also evaluated modeling the slope before and after its construction.

Finally, unidimensional creep constitutive models of the rocks were used to characterize the kinematic evolution of the Shadong landslide in Gongjue County, Tibet, China (Liu et al. 2021). These models enable us to explore the creep behaviors of landslides. As it is well known, three main phases can be differentiated in the creep acceleration of a landslide (Dai et al. 2020; Liu et al. 2021; Xu et al. 2011): primary, secondary, and tertiary creep. During the primary creep, the transient decelerating creep strain rate of

the landslide gradually decreases over time during a short period roughly following a logarithmic law. Secondary creep typically presents slow movements at a nearly constant rate (i.e. nearly constant velocity) that can be strongly influenced by external actions such as earthquakes and rainfall. It should be noted that secondary creep can last from months to decades. Finally, during tertiary creep (also called hyperbolic acceleration) a quick acceleration of the displacements occurs until the final rupture of the slope.

Lomnitz (1956; 1957), proposed next equation, which fits the evolution over time (t) of the displacements (d) during the primary stage of creep of a landslide:

$$d = A \cdot \ln(1 + \alpha \cdot t) \quad (6)$$

where A and α are constants.

Similarly, the primary and secondary stages of creep roughly follow the next equation (Aydan et al. 2013):

$$d = A + B \cdot \log(t) + C \cdot t \quad (7)$$

where A , B and C are constants of the model.

Aydan et al. (2013) proposed next equations which can be used to reproduce all creep stages:

$$d = A \cdot \left(1 - e^{-\frac{t}{\tau_1}}\right) + B \cdot \left(e^{-\frac{t}{\tau_2}} - 1\right) \quad (8)$$

where A , B , τ_1 and τ_2 are constants of the model.

Finally, Aydan et al. (2013) recommended the use of the model proposed by Griggs and Coles (1954) to reproduce the tertiary stages of creep:

$$d = A + B \cdot t^2 \quad (9)$$

where A and B are constants of the model.

3.6. Application of InSAR-based landslide early warning system

Early warning systems look for to determine where and when slopes are likely to fail. InSAR enables the identification and monitoring of landslides and plays a key role in the early warning of these geohazards (Dai et al. 2020). As explained in the previous section, three main steps can be differentiated in creeping landslides (Dai et al. 2020; Liu et al. 2021).

Xu et al. (2011) proposed a method based on the evaluation of the changes in the displacements of the landslides over time, compared to baseline estimates of the steady-state creep rate during secondary creep. The parameter used to assess the changes in the evolution of the landslide is the tangential angle (α) that represents the angle between the tangent of the displacement-time curve and the horizontal axis at a given time (Fan et al. 2019; Xu et al. 2011):

$$\alpha = \text{atan}\left(\frac{v}{v_0}\right) \quad (10)$$

where v_0 is the steady-state creep rate during the secondary creep stage and v is the displacement rate change with unitary measurement time.

According to Xu et al. (2011) and Fan et al. (2019), if $\alpha < 45^\circ$, the landslide lies into the primary creep stage and the early warning level is “secure”; when $\alpha \sim 45^\circ$, the landslide goes into the secondary creep phase, exhibiting constant deformations and an early warning level of “attention”; and if $\alpha > 45^\circ$, the landslide goes into the tertiary creep. More specifically, for α values higher than 45° these authors observed that the deformations of the landslide significantly increase for α values between 45 and 80° (initial acceleration with a level of early warning of “caution”), that it presents impending signals of failure, and sharply increases the velocity of the landslide for α values between 80° and 85° (medium-term acceleration with

a level of early warning of “vigilance”). Finally, the landslide reaches a values near 89° just before failure.

In this DRAGON project, the above-described method was applied to analyze the acceleration process of the Laojingbian landslide using long-term displacement time series derived from the SAR offset tracking method in order to define an early warning.

4. The project’s outputs

The main outputs of this DRAGON project obtained from the application of the methodologies described in subsections 3.1 to 3.6 are presented in section 4.1 to 4.6, respectively, to facilitate the presentation of the results.

4.1. Procedure for phase unwrapping errors and tropospheric delay correction

Figure 4 shows two examples of unwrapped interferograms obtained from PAZ images (X-band) before

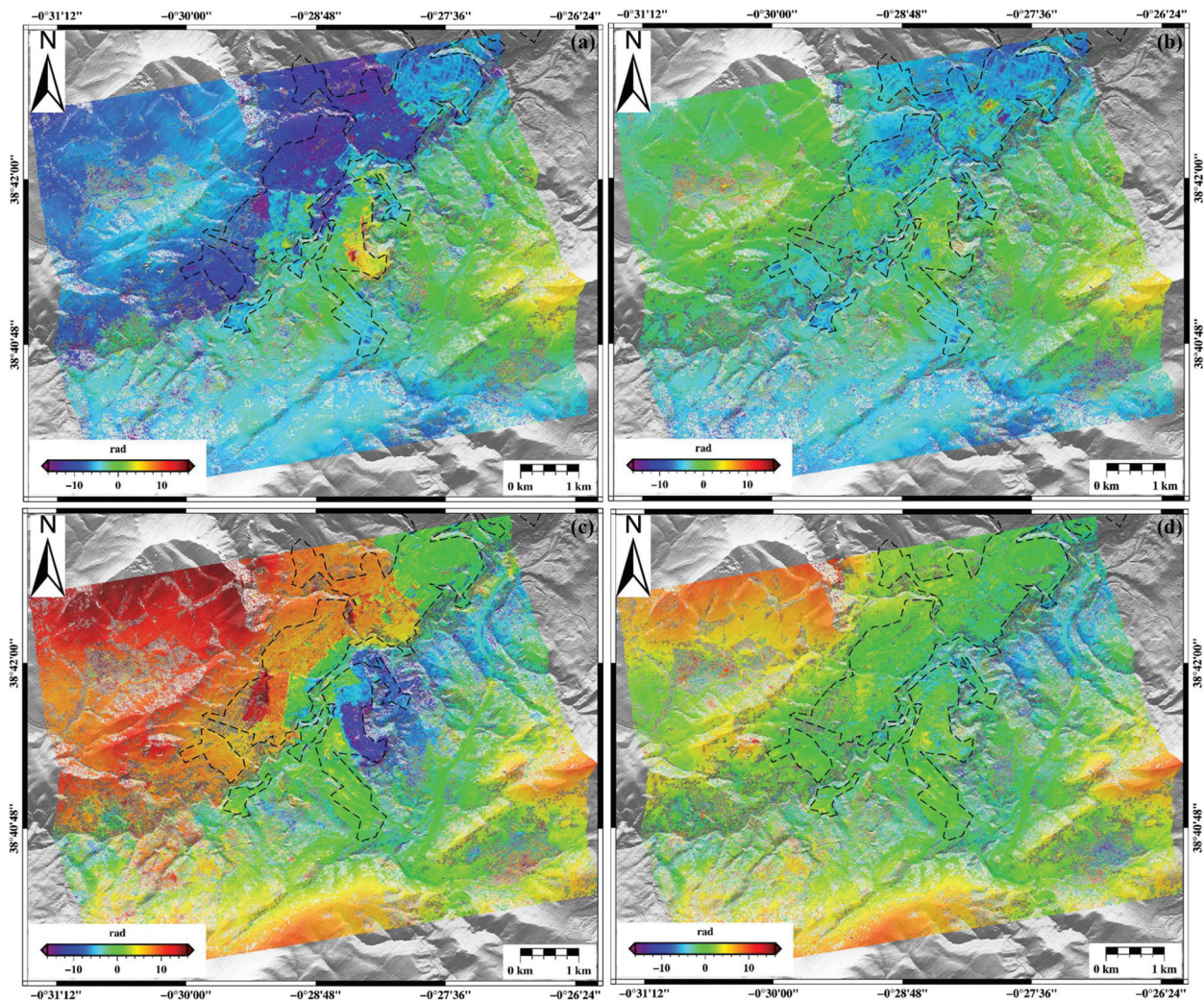


Figure 4. Unwrapped interferograms of Alcoy without and with correction of phase unwrapping errors. (a) and (c) are the unwrapped interferograms before correcting unwrapping errors for pairs 20 September 2019 with 25 November 2019 and 12 October 2019 with 17 December 2019, respectively; and (b) and (d) are the corresponding unwrapped interferograms after correcting unwrapping errors.

and after correcting phase-unwrapping errors with the proposed method in Alcoy (Spain). As it can be clearly observed in the original unwrapped interferograms, shown in Figure 4(a,c), pixels in building areas (see the dotted lines in Figure 1) and vegetated areas are severely contaminated by unwrapping errors, which were caused by dense fringes resulting from physical properties (e.g. expansion and contraction of buildings) as well as decorrelation noise. In comparison, on the examples shown in Figure 4(b,d), the unwrapping errors were efficiently corrected by the threshold detection approach and the combined approach. This result highlights the performance of the proposed approach in correcting phase-unwrapping errors, which is required to accurately retrieve the ground displacement using high-resolution SAR images.

Figure 5 shows an exemplary unwrapped interferograms corrected by different approaches for atmospheric delays. It can be found from Figure 5(a) that the original interferometric phases are strongly impacted by atmospheric delay, with a standard deviation of 4.12 rad. The standard deviation after the GACOS correction is 4.03 rad. The phase-based correction model is slightly better than the GACOS correction, providing a standard deviation of 3.35 rad. Figure 5(d) presents the results after atmospheric delay corrections with both the phase-based and the quadratic model, where the quadratic model was applied to the entire image. We can see that the quadratic model estimates the regional patterns of long-wavelength artifacts well, and the standard deviation

decreases to 2.52 rad for the interferogram. However, this correction introduces some large residuals in localized areas. Finally, the proposed approach improves the atmospheric delay correction compared to the GACOS and the phase-based approaches (see Figure 5(e)), and the standard deviation is reduced to 1.02 rad.

4.2. Improvement of a cross-platform SAR offset tracking method for the retrieval of ground displacements

The Laojingbian landslide in the Wudongde Reservoir Area, situated along the Jinsha River in China, is employed as a case study to illustrate the proposed cross-platform Synthetic Aperture Radar (SAR) offset-tracking method using ALOS/PALSAR-1 and ALOS/PALSAR-2 images acquired between 27 August 2007 and 15 May 2020. Figure 6 shows the two-dimensional (2D) annual displacement rates of the Laojingbian landslide in the azimuth and slant-range directions retrieved from the proposed cross-platform SAR offset-tracking method. The blue colors in Figure 6(a) indicate that the pixels are moving along the flight direction of the satellites, and the blue colors in Figure 6(b) indicate that the landslide is moving away from the satellites. We can see from Figure 6 that the landslide movements were simultaneously measured in both the azimuth and slant-range directions, suggesting that the Laojingbian landslide has 3D movement characteristics. The maximum

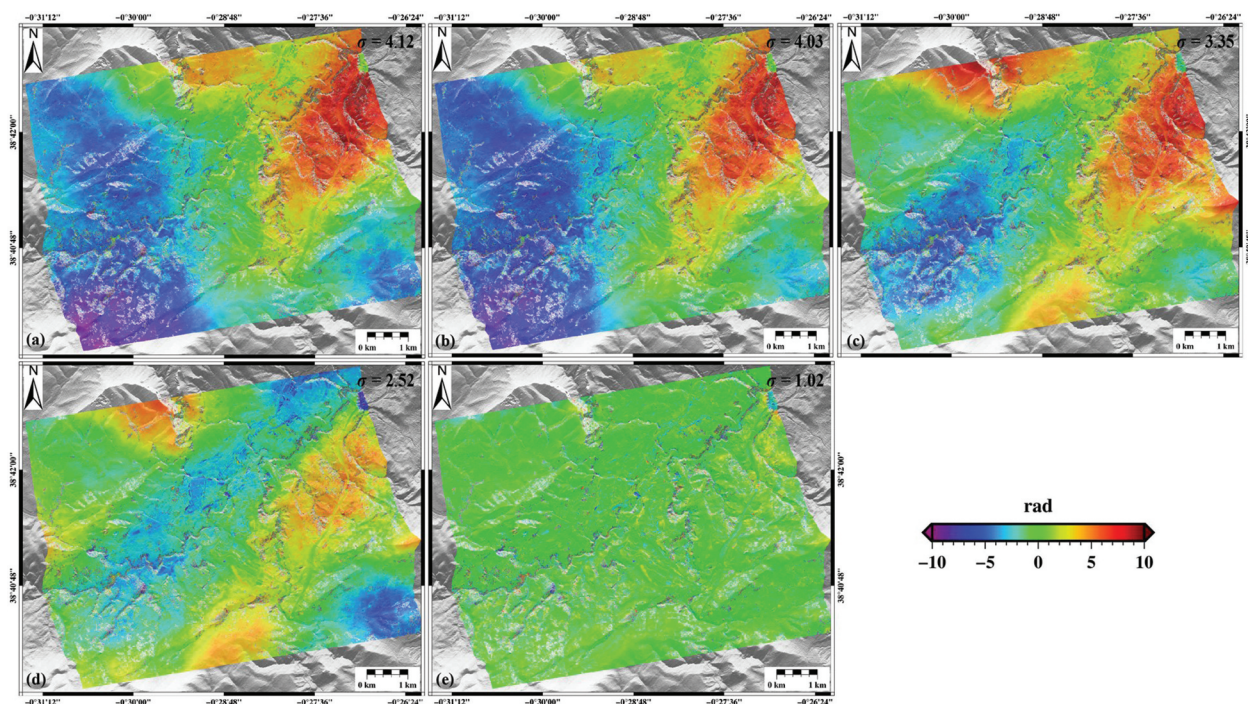


Figure 5. Unwrapped interferogram (24-jul-2020 with 15-aug-2020) of Alcoy with atmospheric delays corrected by different approaches: (a) original uncorrected interferogram; (b) correction using the GACOS product; (c) correction using the phase-based model; (d) correction using the phase-based model and the quadratic model over the entire image; and (e) correction using the proposed approach.

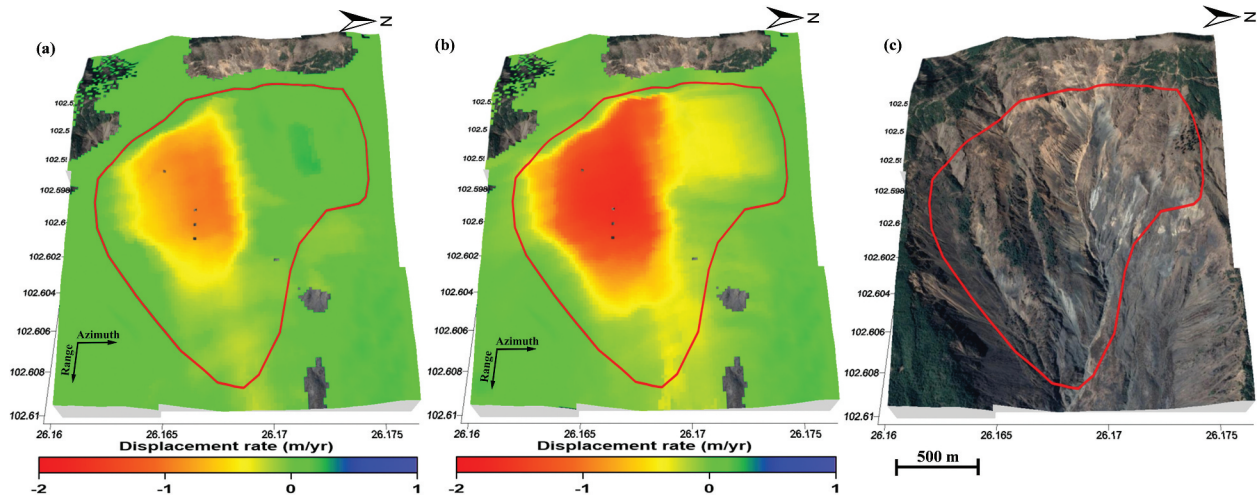


Figure 6. Two-dimensional (horizontal) displacement rates of the Laojingbian landslide in the azimuth (a) and slant-range (b) directions, respectively, retrieved from the cross-platform ALOS/PALSAR-1 and ALOS/PALSAR-2 images between August 2007 and May 2020 (modified from Liu et al. 2021). Note that the negative values in (a) indicate movement of the pixels along the flight direction of the satellites (azimuth), while the negative values in (b) indicate movement of the landslide away from the satellites. Conversely, positive values indicate movement in the opposite directions.

displacement rate in the azimuth direction from August 2007 to May 2020 was -1.0 m/year, and the corresponding displacement rate in the slant-range direction was -1.7 m/year. The results suggest that the landslide movement in the slant-range direction is approximately 1.7 times that in the azimuth direction. The average slope aspect derived from DEM indicates that the Laojingbian landslide is oriented toward the east, which is nearly perpendicular to the flight directions (approximately -10° from the north) of the ALOS/PALSAR-1 and ALOS/PALSAR-2 sensors. Thus, the observed landslide displacement mainly occurred in the slant-range direction.

On the basis of the 2D displacement rates presented in Figure 6, we can observe a clear boundary of the maximum displacement regions (see the left slope). This finding demonstrates that the SAR offset tracking method has the potential to map the most active part of a landslide compared to the traditional InSAR

techniques, which exhibit significant limitations in the capability to measure large-gradient deformation due to the ambiguous nature of the observations.

4.3. Polinsar monitoring of landslides

Figure 7 shows the histograms of the estimated DEM error and linear velocity in different PS groups (Luo et al. 2022). We can see that, in the VV channel, neither the DEM error nor the linear velocity follows a Gaussian distribution with zero-mean, whereas the OPT channel provides distributions whose average is closer to zero than with the VV channel. The lower density of pixels and the sparse network built by linking pixels of the VV channel make it less reliable than the OPT channel.

The linear velocity map is given in Figure 8. As it can be seen, the deformation areas measured by the VV channel are quite isolated. However, after using

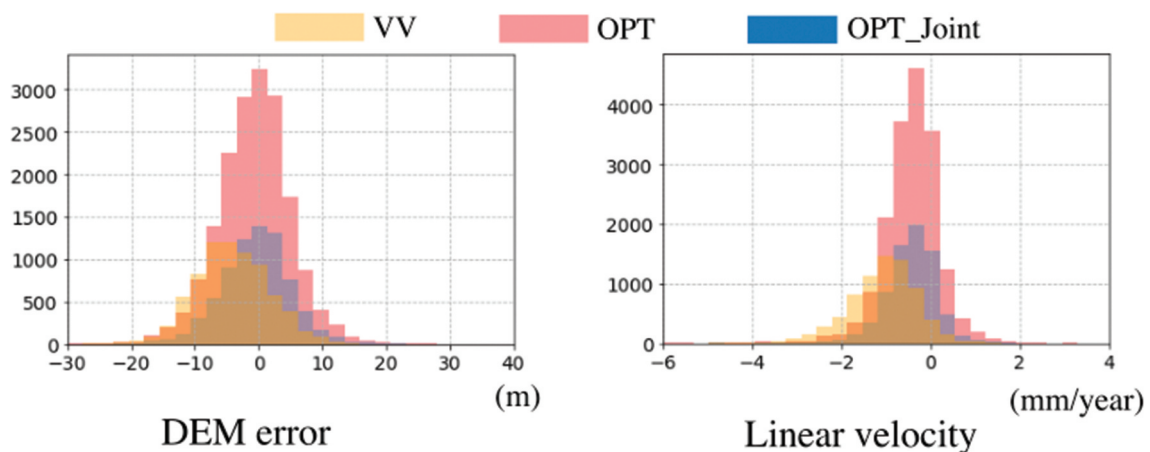


Figure 7. Histograms of estimated linear velocity and DEM error for PS points selected in VV or OPT channels over Alcoy, Spain. Joint means PS points selected in both VV and OPT channels.

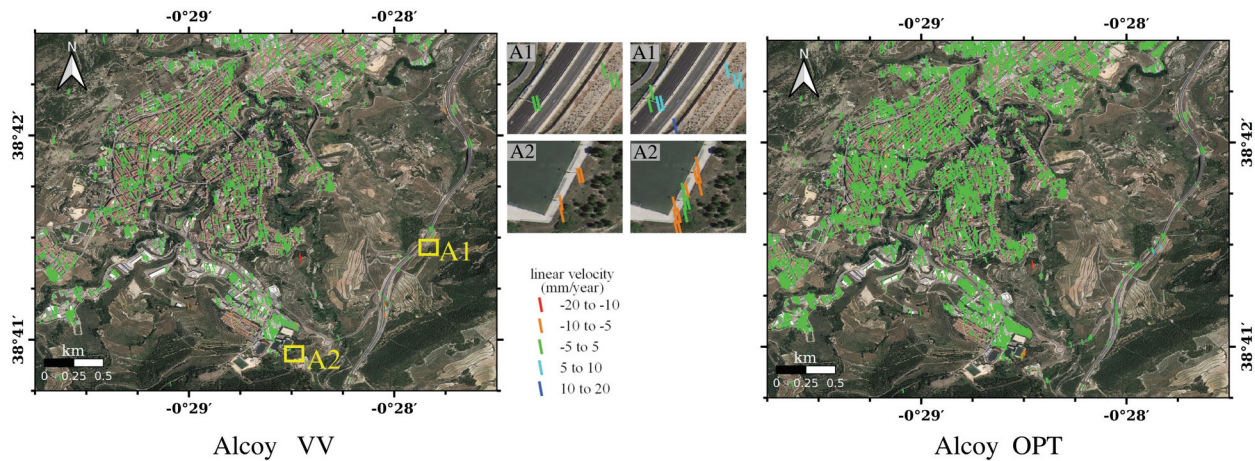


Figure 8. Linear velocity maps for VV and OPT channels over Alcoy, Spain (modified from Luo et al. 2022).

the OPT channel, the density of PS points has considerably increased, with its total number going from 4158 to 10,351. Due to the increased PS points, the deformation estimates are more reliable. For example, in area A1, the deformation rates do not exceed 5 mm/year for the VV channel. However, the in-situ displacement rate is 10.04 mm/year, which is very similar to the value obtained from the OPT channel. In area A2, the OPT channel can provide additional measurement points over a landslide zone already detected by the VV channel, thus increasing the detection area for this landslide.

4.4. Semiautomatic mapping of active deformation areas on wide regions

ADAfinder enables us to automatically map Active Deformation Areas (ADA) from large InSAR datasets. The capability of this approach has been proved through its application to the mining area of La Unión, Alcoy and Deqin.

In La Unión, 28 and 19 ADAs were automatically mapped from the ascending and descending displacement rate datasets of the period comprised between October 2016 and November 2021 (Hu et al. 2023). Nineteen and 10 of these ADAs out of the total number of ADAs corresponded to landslides. Figure 9 shows two examples of active deformation areas (ADA) associated with landslides in La Unión. As it can be seen, first, the active areas are automatically delineated by ADAfinder for each independent dataset (i.e. for ascending and descending datasets). Second, the ADAs associated to landslides were identified considering the previous existing landslides' inventory map and the safety factor values (Figure 9(c,d)). Then, the contours of the ADAs derived from different sources (i.e. the InSAR and the inventory map) were merged to define the actual contour of each ADA (Figures 9(a,b)). Finally, the landslides are confirmed with the support of aerial optical images (Figure 9(e,f)) and fieldwork.

In the mountain region of Deqin, a total of 317 ADA associated to landslides were automatically mapped using the improved ADAfinder approach described in section 3.4. Then, the obtained ADA were classified with the support of an existing landslides' inventory map and the analysis of geomorphological features through high-resolution images and a digital elevation model acquired by an unmanned aerial vehicle. As a result, 258 landslides were classified as flows, 25 as falls and 34 as slides.

4.5. Modelling and identification of triggering factors of landslides

The application of the infinite slope stability model to the mining area of La Unión enabled the identification of those areas with a safety factor lower than 1 (i.e. unstable). The map of the distribution of the safety factor for $D = 30$ m and $H_w = 0$ (i.e. dry conditions) is shown in Figure 9(a), showing a total unstable area of more than 1 million square meters, and an area higher than 1.2 million square meters with a critical safety factor (i.e. between 1.0 and 1.2). The safety factor values lower than 1 mostly concentrate on the slopes of the mining waste dumps and to a lesser extent on some open-pit slopes. It is worth noting that this information is independent of InSAR data (i.e. it is an external information) and has been used as ancillary information to preliminarily classify the active deformation areas delineated by InSAR, assuming that those active deformation areas detected by InSAR and associated to a landslide would exhibit low slope safety factors as it can be seen in landslides 67 and 68 shown in Figure 9. These landslides were contained in an existing inventory map of landslides of the mining area of La Unión but were automatically delineated, and thus confirmed as active landslide, by InSAR data derived from Sentinel-1 between 2015 and 2022. The safety factor map in this area shows an important concentration of values lower than 1,

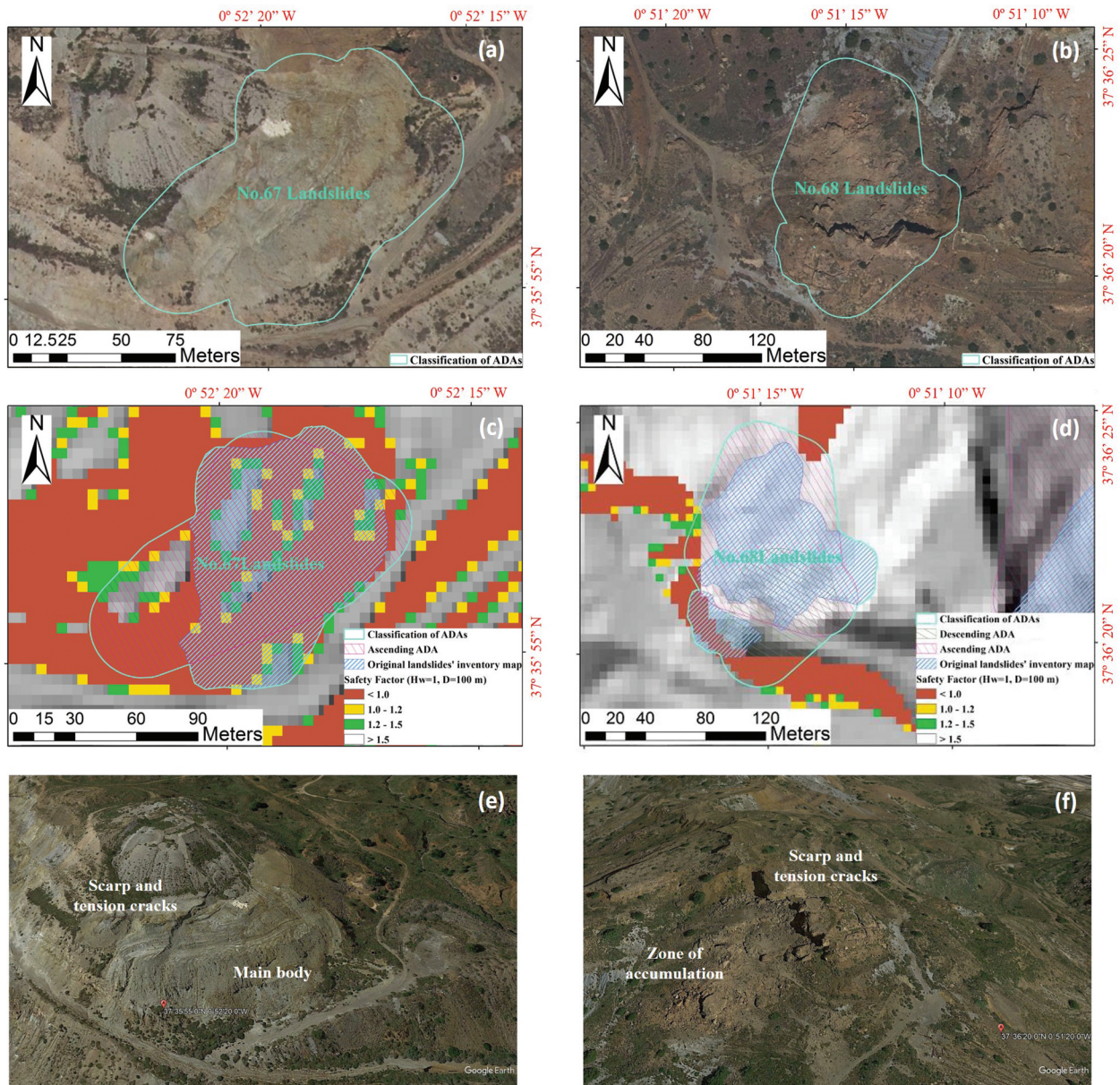


Figure 9. Example of two active deformation areas associated to landslides nº 67 and 68 automatically mapped by ADAfinder from InSAR data in the mining area of La Unión. (a) and (b) represent the ADA contours resulting from merging the previously existing landslides' inventory map and the InSAR-derived ADAs. (c) and (d) Safety factor's maps and ADAs automatically detected by InSAR and ADAs included in the original landslides' inventory map. The meaning of variables H_w and D is defined in Section 3.5. (e) and (f) Oblique aerial images of the landslides.

confirming the precarious equilibrium of these slopes. Consequently, this case demonstrates the usefulness of the use of a simple infinite slope stability model as ancillary information to classify active deformation areas delineated by InSAR.

In Alcoy, a 3D probabilistic numerical model was used to evaluate the equilibrium conditions of a landslide affecting an important transportation route and to identify the triggering factors of the slow-moving landslide, as explained in section 3.5 (Tomás et al. 2023). The results are summarized in Figure 10(b). As it can be seen, the safety factor strongly depends on the hydraulic conditions of the slope, represented by the factor r_u shown in the X-axis. The higher the r_u value (i.e. the more saturated the

slope due to rainfall), the lower the safety factor and the higher the probability of failure of the slope, confirming the close relationship between rainfall and InSAR measured displacements observed in this landslide by Szeibert et al. (2022) and Tomás et al. (2023). Additionally, the influence of the construction of an embankment at the head of the landslide to eliminate the existing curve of the road was analyzed. To this aim, the slope was modeled “with” and “without” embankment. The results are also depicted in Figure 10(b) and show a clear reduction of the safety factor and an increase in the probability of failure when the construction of the embankment is considered, in agreement with the InSAR displacement distribution that shows a concentration of displacements

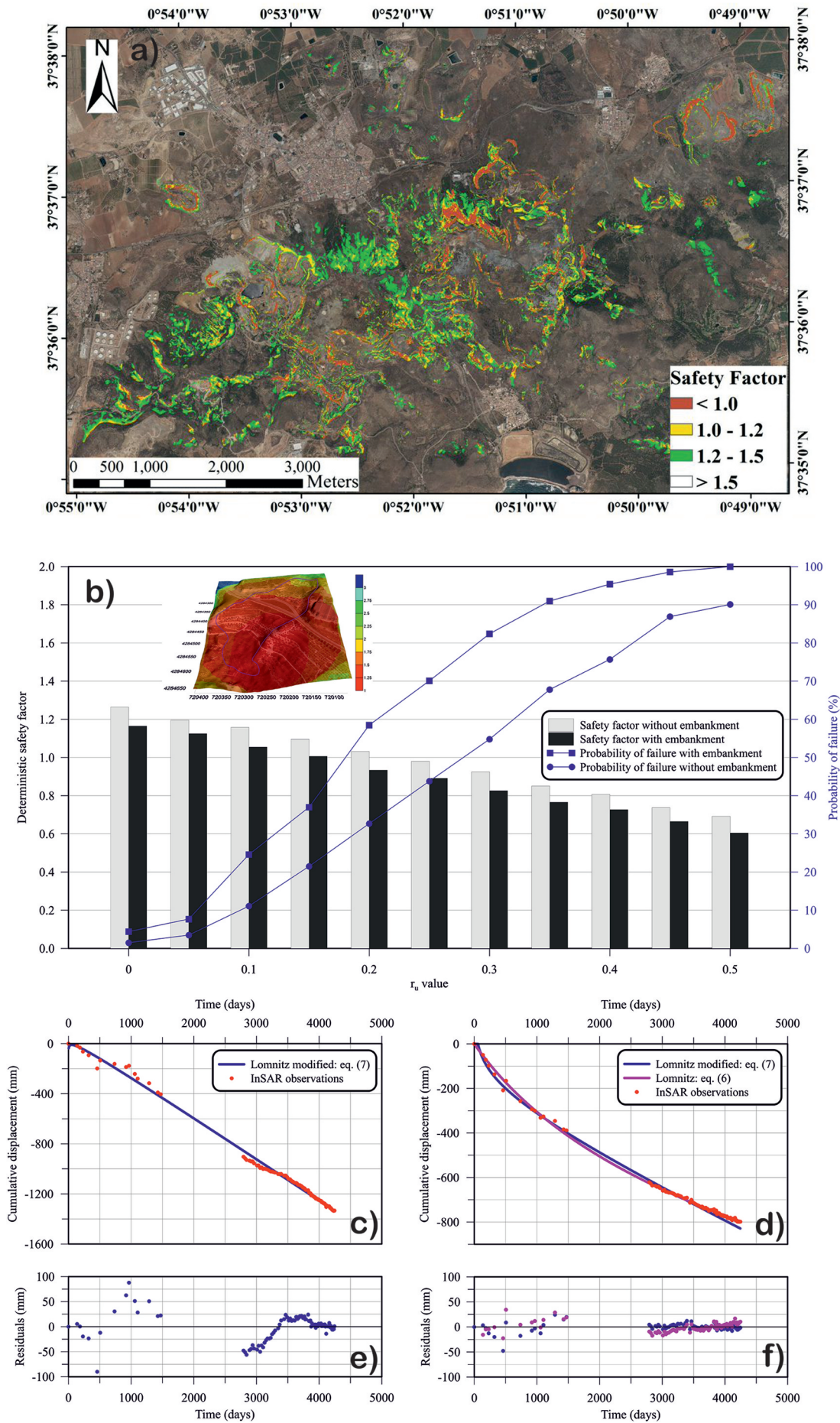


Figure 10. (A) Safety factor map of La Unión (Spain) computed by means of an infinite slope failure for $D=30\text{ m}$ and $H_w=0$ used for the preliminary classification of ADAs detected by InSAR. (b) Variation of the deterministic safety factor and the probability of failure vs the r_u values of a slow-motion landslide monitored by InSAR in Alcoy (Spain) before and after the construction of an embankment. (c) Fitting of unidimensional constitutive creep models defined by Equation 6 and Equation 7 to InSAR time series of Shadong landslide in Gongjue County (China). P1 and P3 show a secondary and primary creep behaviours, respectively.

over the embankment (Szeibert et al. 2022; Tomás et al. 2023). Therefore, the developed numerical model has contributed to the interpretation of the InSAR results on a slow-moving landslide, as well as to the identification of the main triggering factors by cross-analyzing InSAR and modeling data.

In the Shadong landslide in Gongjue County, Tibet (China), ALOS/PALSAR-1 (L-band) and Sentinel-1 (C-band) SAR images were linked by means of the Tikhonov Regularization (TR) method to define a 12 years of displacement time series (Liu et al. 2021). Unidimensional constitutive creep models (Aydan et al. 2013) of rocks described in section 3.5 were then applied to reproduce the measured displacements (Figure 10(c,d)). The results show that the creep model fits well to the InSAR data. It means that the Shadong landslide exhibits a creep behavior. In detail, the results show that some points as P3 fit very well Equations (6) and (7) and exhibit a clear non-linear trend, indicating that the landslide is deforming under a primary creep stage. In contrast, other points as P1 perfectly fits the model defined by Equation (7) but fails when trying to fit the other creep laws defined in 3.5 and defined a linear-like behavior, suggesting that this area has entered into secondary creep. Moreover, the analysis of Figure 10(e,f) enables to observe that the highest residue is located on 22 May 2008, very close in time to the occurrence of the 2008 Wenchuan earthquake (M_w 7.9) which hit this area on 12 May 2008. Therefore, the displacement anomaly of the Shadong landslide (i.e. the deviation of the displacements from the theoretical creep law)

observed in May 2008 could be related to the effect exerted by the earthquake on the landslide. Hence, this case study has highlighted the utility of rock creep models to identify the creep stage of creeping landslides as well as to identify abnormal behaviors induced by external forces such as earthquakes.

4.6. Application of InSAR-based landslide early warning system on selected sites

Figure 11 shows the time series of the horizontal displacements of a representative point placed on the main body of the Laojingbian landslide from August 2007 to May 2020 obtained through the combination of the E-W and N-S components calculated by Yin et al. (2022).

The analysis of the time series enables the differentiation of two different stages of deformation. First, from August 2007 to February 2015 a horizontal displacement rate near 4.3 mm/day was measured. Second, the Laojingbian landslide exhibited a horizontal displacement rate of 11.3 mm/day between February 2015 and May 2020.

The tangential angle was then calculated for the second period of the time series comprised between February 2015 and May 2020 using Equation (10), providing values higher than 68° . This tangential angle is higher than 45° and lower than 80° , indicating that the Laojingbian landslide has entered into an “initial accelerative deformation” according to the thresholds defined by Xu et al. (2011) and Fan et al.

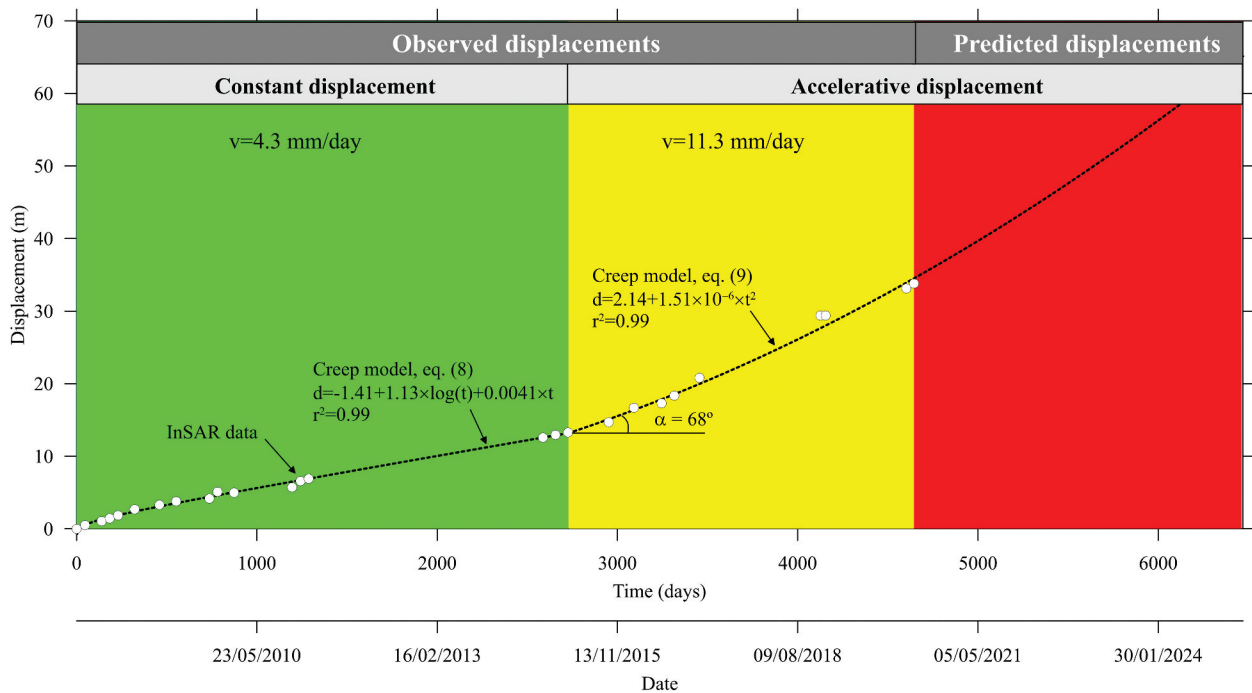


Figure 11. Creep models (black thick dashed line) fitted to the horizontal 3D displacements (white dots) derived from SAR offset tracking of a point placed on the area of maximum deformation of Laojingbian landslide from August 2007 to May 2020. v , r^2 and α are the mean displacement rate, the coefficient of determination and the tangential angle, respectively.

(2019). Therefore, a yellow warning, which entails a caution level, should be issued to the Laojingbian landslide.

Furthermore, unidimensional creep models described by Equations (7) and (9) have been successfully fitted to reproduce the period of constant and accelerative displacements, respectively, providing a coefficient of determination (r^2) of 0.99 (Figure 11). It is worth noting that, as was described in section 3.5, Equation (7) is suitable to reproduce the primary and secondary creep deformations, while Equation (9) enables to reproduce tertiary creep. Therefore, the equation fitted to the horizontal displacements measured during the accelerative displacement stage suggests that the Laojingbian landslide will reach up to 65 m in 2025 under natural conditions, although these values may be even higher due to extraordinary rainfall periods or earthquake events. Therefore, a detailed real-monitoring and early warning system must be implemented in Laojingbian landslide to avoid, or at least to minimize the impact imposed by the eventual failure of the landslide.

5. Discussion and conclusions

This work summarizes the advances obtained during the first 2 years of the DRAGON-5 project ID 59,339 regarding the investigation of landslides in different areas of study and contexts by space-borne synthetic aperture radar interferometry.

The first achievement of the project shown in this paper consisted in the development of a procedure for correcting phase-unwrapping errors and tropospheric delays. Regarding the unwrapping errors, this approach combines spatial and temporal information to perform the correction of the interferograms. To this aim, on the one hand, obvious phase-unwrapping errors are first corrected in the interferograms by means of the use of spatial-domain information. On the other hand, the principle of the consistency of triplets of interferometric phases is used in the temporal domain to correct phase unwrapping errors (Yunjun, Fattahi, and Amelung 2019). Complementarily, a block-based correction approach was proposed for atmospheric delay correction. This procedure encompasses the decomposition of the principal component analysis, the masking of the active deformation areas, the estimation of the atmospheric artifacts and the calculation of the corrected displacements. The results obtained in Alcoy using high-resolution PAZ images show a reduction of the total standard deviation of 37.7% on average over 50 selected interferograms and an average inner precision of the estimated displacement of 44% against the GACOS and phase-based methods, demonstrating the proper function of the proposed methodology.

Another notable accomplishment involved the enhancement of a cross-platform SAR offset tracking method for the measurement of two-dimensional ground displacements in the azimuth and slant-range directions. As it is well known, SAR offset tracking is a powerful tool for mapping large-gradient landslide displacements in both the slant-range and azimuth directions using images acquired by the same satellite. However, the main novelty of the developed approach consists in the capability of the new method to calculate the two-dimensional offsets between SAR images not only from an identical platform (e.g. ALOS-1 and ALOS-1) but also from cross platforms (e.g. ALOS-1 and ALOS-2). In the DRAGON project, the methodology has been successfully applied to the Laojingbian landslide, measuring horizontal displacement rates in the azimuth and slant-range directions of -1.0 and -1.7 m/year, respectively, between August 2007 and May 2020. In conclusion, this approach signifies a remarkable improvement to overcome the intrinsic limitations of traditional InSAR techniques to monitor large-gradient landslides.

A third achievement is related to the application of polarimetric SAR interferometry to monitor active landslides. This technique was successfully applied to Alcoy using 186 Sentinel-1 images captured between January 2017 and January 2021. The results showed a significant increase in the number of coherent pixels when using the OPT channel, from 4158 to 10,351 (i.e. an increase of 148%). Therefore, due to the increase in the number of PS points, a more reliable estimation of the ground surface displacements is expected. Summarizing, the higher density of points increases the capability of PolInSAR to detect and monitor landslides within areas in which a low density of points or no points are provided by conventional PSInSAR techniques.

In this DRAGON project, semiautomatic processes for mapping active displacement areas in wide regions have also been applied and adapted. ADAfinder has been successfully used in La Unión to elaborate a map of active deformation areas. This map has been subsequently classified based on a spatial slope stability model. In Deqin, the process of identification of ADAs has been slightly modified in order to increase the efficiency of the processing of wide areas. Additionally, the C-index and the quality index have been considered in order to classify the reliability of the ADAs. In short, this method considerably facilitates the supervised analysis of large InSAR datasets, enabling the extraction and delineation of active deformation areas and contributing to their preliminary classification and interpretation. It should be noted that this type of tool is especially relevant in the present context, in which huge InSAR regional and nation-wide datasets are becoming more common (Crosetto et al. 2020).

In relation to modeling, different experiences have been developed. The great value of the joint use of

geotechnical models and InSAR datasets has been demonstrated in the mining area of La Unión and in Alcoy. In this study area, a simple deterministic model based on external geotechnical and geomorphological information has been used to evaluate the spatial stability conditions of the area of interest. The obtained safety factor maps, jointly with optical images, have enabled the subsequent pre-classification of the active deformation areas automatically delineated based on InSAR datasets. The final active deformation maps provide a valuable information for land managers, since they depict an actual picture of the existing active processes, enabling the identification of potential areas of risk for the population and the subsequent implementation of complementary in situ monitoring systems.

The potential of numerical models to evaluate the stability of landslides has also been confirmed in Alcoy. The joint analysis of InSAR data and the model has allowed the characterization of the kinematics of the landslide, as well as the identification of rainfall and the construction of an embankment on the head as the main triggering factors of this slow-moving landslide. Both factors reduce the safety factor of the slope and increase the probability of failure. This information, jointly with other complementary in situ geotechnical works, can be crucial for an efficient design of corrective measures of the slope.

Furthermore, the creep behavior of Laojingbian landslide, in Wudongde reservoir, monitored during nearly 8 years has been characterized and reproduced using unidimensional creep models of rocks. The fitted functions have permitted to identify different types of creep stages and to issue a yellow early warning based on the tangential angle, a parameter derived from the InSAR time series. Moreover, the model has been used to predict future deformations, which will reach near 65 m in 2025.

In conclusion, the results achieved in the framework of the DRAGON project during last 2 years, which are mainly focused on selected sensitive regions in Spain and China and different topics related to processing and application of InSAR, provide essential assets for planning present and future scientific activities devoted to identify, map, characterize, monitor and predict landslides, as well as for the implementation of early warning systems. Therefore, the performed analyses are crucial for an optimal prevention and management of these destructive and dangerous geohazards. However, further research and development are needed to refine and expand the application of the methodologies developed in the DRAGON project. Additionally, addressing the limitations and shortcomings identified in the current findings, such as the need of fully automatic ADAs' classification processes based on multivariate statistical algorithms or machine learning techniques, the

determination of 3D time-series displacement components of slow- and rapid-moving landslides using InSAR and SAR offset-tracking data by assuming different failure modes, the prediction of landslide displacements with InSAR and SAR offset-tracking time series using machine learning techniques, or the evaluation of the capabilities of PolInSAR to monitor landslides in non-urban areas, will be crucial for enhancing the accuracy and reliability of landslide identification, mapping, characterization, monitoring, and prediction, as well as for the implementation of more effective early warning systems.

Acknowledgment

All the PAZ images were provided by INTA (National Institute of Aerospace Technology) as part of PAZ-Ciencia (Scientific Exploitation of PAZ, project nr. PAZ-AO-001-025) and the Sentinel-1 datasets used in this study were freely downloaded from Copernicus and ESA.

Disclosure statement

No potential conflict of interest was reported by the author(s).

Funding

This work was supported by the ESA-MOST China DRAGON-5 project with ref. 59339, by the Spanish Ministry of Science and Innovation, the State Agency of Research (AEI), and the European Funds for Regional Development under grant [grant number PID2020-117303GB-C22], by the Conselleria de Innovación, Universidades, Ciencia y Sociedad Digital in the framework of the project CIAICO/2021/335, by the Natural Science Foundation of China [grant numbers 41874005 and 41929001], the Fundamental Research Funds for the Central University [grant numbers 300102269712 and 300102269303], and China Geological Survey Project [grant numbers DD20190637 and DD20190647]. Xiaojie Liu and Liuru Hu have been funded by Chinese Scholarship Council Grants Ref. [grant number 202006560031] and [grant number 202004180062], respectively.

Notes on contributors

Roberto Tomás received the Tech. Eng. (B.S.) degree in civil engineering, the M.S. degree in civil engineering, the M. S. degree in geological engineering, and the Ph.D. degrees in earth sciences and geological engineering from the University of Alicante (UA), Alicante, Spain, in 1998, 2002, 2007, and 2009, respectively. He is currently a full professor in the Department of Civil Engineering in the UA. His research interests include the application of remote sensing techniques for monitoring and modeling of natural hazards (with emphasis on landslides and land subsidence) and infrastructure, as well as for rock mass characterization.

Qiming Zeng received the B.S. degree in physics, the M. S. degree in cartography and remote sensing, and the

Ph.D. degree in cartography and remote sensing from Peking University, Beijing, China, in 1985, 1988, and 2001, respectively. In 1988, he joined the Institute of Remote Sensing and Geographic Information System, Peking University, where he is currently a professor. His research interests include microwave remote sensing, particularly those using synthetic aperture radar data.

Juan M. Lopez-Sanchez is a full professor at the Institute for Computer Research (IUII), University of Alicante, Spain. He received the PhD degree from the Technical University of Valencia in 2000. His research interests include radar remote sensing processing and advanced techniques, as well as applications in agriculture and geophysics.

Chaoying Zhao is a professor of geodesy and survey engineering with Chang'an University. He received his M.S. and Ph.D. degrees in geodesy and surveying engineering from Chang'an University, Xi'an, China, in 2002 and 2009, respectively. His research interests include the development of different InSAR methods and their applications in geohazard identification, monitoring, and mechanism explanations.

Zhenhong Li is a professor of imaging geodesy with the College of Geological Engineering and Geomatics, Chang'an University, Xi'an, China, and Vice Director of Key Laboratory of Loess, Xi'an, China. He received the B. Eng. degree in geodesy from the Wuhan Technical University of Surveying and Mapping (now Wuhan University), Wuhan, China, in 1997, and the Ph.D. degree in GPS, geodesy, and navigation from University College London, London, UK, in 2005. His research interests include imaging geodesy and its applications to geohazards (e.g., earthquakes, landslides, and land subsidence) and precision agriculture.

Xiaojie Liu received the M.Sc. and Ph.D. degrees in surveying and mapping from Chang'an University, China, in 2018 and 2022, respectively, and the PhD degree in Geological Engineering from the University of Alicante, Spain, in 2023. He is a lecturer at the School of Civil Engineering in surveying and mapping, Lanzhou University of Technology, Lanzhou, China. His research interests include interferometric synthetic aperture radar and its applications in large-area landslide detection, monitoring and mechanism analysis.

María I. Navarro-Hernández received her Bachelor's Degree in Engineering Geology from the National University of Colombia, and her Master's Degree in Technology and Water Management from the Autonomous University of San Luis Potosí (Mexico) in 2020. Currently, she is conducting a PhD at the University of Alicante (Spain). Her experience is related to the interpretation of SAR Interferometry (InSAR) data for the analysis and monitoring of land subsidence in overexploited aquifer systems, estimation of hydrogeological parameters and validation with GNSS technology

Liuru Hu is a PhD at the University of Alicante. She received her B.E. and M.Sc. degrees in Remote Sensing and Photogrammetry from the Chang'an University and Shandong University of Science and Technology in 2013 and 2017. Her research interests lie in the field of semi-automatic identification and monitoring of large-area landslides with InSAR and multi-source data.

Jiayin Luo received the B.S. degree in Geomatics Engineering from the Northeastern University, Shenyang, China, in 2018, and the M.S. degree in Geomatics Engineering from the State Key Laboratory of Information Engineering in Surveying, Mapping and Remote Sensing, Wuhan University, China, in 2020. She is currently pursuing the Ph.D. degree in Computer Science at the University of Alicante, Spain. Her research interests include polarimetric and interferometric techniques.

Esteban Díaz is an associate professor at the University of Alicante (Spain), where he received a Ph.D. degree in 2015. His primary areas of research encompass numerical modeling, machine learning, AI techniques, and geotechnical engineering.

William T. Szeibert is an InSAR post-processing specialist working at Sixense Iberia's satellite department. He received his M.Sc in engineering geology from the University of Alicante in 2022. His research interests include slope stability detection and analysis via remote sensing methodologies.

José Luis Pastor is an associate professor at the Department of Civil Engineering of the University of Alicante (Spain). He received his PhD degree from the University of Alicante in 2016. His research interests include soil improvement, settlements and soil mechanics

Adrián Riquelme is an associate professor in the Civil Engineering Department at the University of Alicante. He earned his PhD from the University of Alicante in 2015. His main research focuses on utilizing remote sensing datasets for characterizing discontinuity sets in rocky slopes.

Chen Yu is a professor at the College of Geological Engineering and Geomatics, Chang'an University, Xi'an, China. He received his PhD from Newcastle University in the UK. He majors in the research of monitoring and interpreting geo-hazards such as earthquakes, volcanoes, landslides, and ground subsidence using a variety of Earth Observations (EO). His main objective is to develop a geohazard Early Warning System (EWS) with the capacity for early-stage hazard detection and pre-warning, risk assessment of the hazard affected area and rapid response to catastrophic events.

Miguel Cano is Ph.D., Civil Engineer (B.Eng.), Geological Engineer (B. Eng. and M.Eng. – 2nd National Award) and Master in Building Construction and Real Estate Management. Currently, he is associate professor in Geotechnical Engineering at the Civil engineering department (University of Alicante). His research interests include the use of remote sensing techniques for geotechnical purposes.

ORCID

Roberto Tomás  <http://orcid.org/0000-0003-2947-9441>
 Qiming Zeng  <http://orcid.org/0000-0003-1020-064X>
 Juan M. Lopez-Sanchez  <http://orcid.org/0000-0002-4216-5175>
 Chaoying Zhao  <http://orcid.org/0000-0002-5730-9602>
 Zhenhong Li  <http://orcid.org/0000-0002-8054-7449>
 Xiaojie Liu  <http://orcid.org/0000-0002-4873-1668>

María I. Navarro-Hernández  <http://orcid.org/0000-0002-8989-3807>
 Liuru Hu  <http://orcid.org/0000-0001-8909-0687>
 Jiayin Luo  <http://orcid.org/0009-0002-0548-3454>
 Esteban Díaz  <http://orcid.org/0000-0003-0799-0484>
 William T. Szeibert  <http://orcid.org/0009-0001-9656-7452>
 José Luis Pastor  <http://orcid.org/0000-0001-7870-3652>
 Adrián Riquelme  <http://orcid.org/0000-0002-2155-3515>
 Chen Yu  <http://orcid.org/0000-0002-9675-8814>
 Miguel Cano  <http://orcid.org/0000-0002-5737-9299>

Data availability statement

The data that support the findings of this study are available from the corresponding author [R.T.], upon reasonable request.

References

- Almela, A., Quintero, E. Gómez-Nogueroles, and H. Mansilla. 1975. "Mapa y memoria explicativa de la Hoja 821 (Alcoy) del Mapa Geológico E. 1: 50.000 Plan Magna."
- Aydan, Ö., T. Ito, U. Özbay, M. Kwasniewski, K. Shariar, T. Okuno, A. Özgenoğlu, D. Malan, and T. Okada. 2013. "ISRM Suggested Methods for Determining the Creep Characteristics of Rock." *Rock Mechanics & Rock Engineering* 47. <https://doi.org/10.1007/s00603-013-0520-6>.
- Barra, A., L. Solari, M. Béjar-Pizarro, O. Monserrat, S. Bianchini, G. Herrera, M. Crosetto, et al. 2017. "A Methodology to Detect and Update Active Deformation Areas Based on Sentinel-1 SAR Images." *Remote Sensing* 9 (10): 1002.
- Biggs, J., and T. J. Wright. 2020. "How Satellite InSar Has Grown from Opportunistic Science to Routine Monitoring Over the Last Decade." *Nature Communications* 11 (1): 3863. <https://doi.org/10.1038/s41467-020-17587-6>.
- Chen, J., F. Dai, T. Lv, and Z. Cui. 2013. "Holocene Landslide-Dammed Lake Deposits in the Upper Jinsha River, SE Tibetan Plateau and Their Ages." *Quaternary International* 298:107–113. <https://doi.org/10.1016/j.quaint.2012.09.018>.
- Colesanti, C., and J. Wasowski. 2006. "Investigating Landslides with Space-Borne Synthetic Aperture Radar (SAR) Interferometry." *Engineering Geology* 88 (3–4): 173–199. <https://doi.org/10.1016/j.enggeo.2006.09.013>.
- Confuorto, P., N. Casagli, F. Casu, C. De Luca, M. Del Soldato, D. Festa, R. Lanari, M. Manzo, G. Onorato, and F. Raspini. 2023. "Sentinel-1 P-SBAS Data for the Update of the State of Activity of National Landslide Inventory Maps." *Landslides* 20 (5): 1083–1097. <https://doi.org/10.1007/s10346-022-02024-0>.
- CRED. 2022. *2021 Disasters in Numbers*. Brussels, Belgium: Centre for Research on the Epidemiology for Disasters.
- Crosetto, M., L. Solari, M. Mróz, J. Balasis-Levinsen, N. Casagli, M. Frei, A. Oyen, et al. 2020. "The Evolution of Wide-Area DInSar: From Regional and National Services to the European Ground Motion Service." *Remote Sensing* 12 (12): 2043.
- Cruden, D. M., and D. J. Varnes. 1996. "Landslide Types and Processes." In *Landslides: Investigation and Mitigation (Special Report)*, edited by A. K. Turner and R. L. Schuster, 36–75. Washington, DC, USA: National Research Council, Transportation and Research Board Special Report.
- Dai, K., Z. Li, Q. Xu, R. Bürgmann, D. G. Milledge, R. Tomás, X. Fan, et al. 2020. "Entering the Era of Earth Observation-Based Landslide Warning Systems: A Novel and Exciting Framework." *IEEE Geoscience and Remote Sensing Magazine* 8 (1): 136–153. <https://doi.org/10.1109/MGRS.2019.2954395>.
- Delgado, J., J. A. Peláez, R. Tomás, A. Estévez, C. López Casado, C. Doménech, and A. Cuenca. 2006. "Evaluación de la susceptibilidad de las laderas a sufrir inestabilidades inducidas por terremotos. Aplicación a la cuenca de drenaje del río Serpis (provincia de Alicante)." *Revista de la Sociedad Geológica de España* 19:197–218. [https://sge.usal.es/archivos/REV/19\(3-4\)/Art3.pdf](https://sge.usal.es/archivos/REV/19(3-4)/Art3.pdf).
- Delgado, J., J. A. Peláez, R. Tomás, C. López-Casado, C. Doménech, A. Estévez, and A. Cuenca. 2004. "Susceptibilidad a movimientos de ladera inducidos por terremotos en Alcoy (Alicante) y sectores adyacentes." *Geotemas* 6:285–288.
- Escobar-Wolf, R., J. D. Sanders, C. L. Vishnu, T. Oommen, and K. S. Sajinkumar. 2021. "A GIS Tool for Infinite Slope Stability Analysis (GIS-TISSA)." *Geoscience Frontiers* 12 (2): 756–768. <https://doi.org/10.1016/j.gsf.2020.09.008>.
- Fan, X., Q. Xu, A. Alonso-Rodriguez, S. S. Subramanian, W. Li, G. Zheng, X. Dong, and R. Huang. 2019. "Successive Landsliding and Damming of the Jinsha River in Eastern Tibet, China: Prime Investigation, Early Warning, and Emergency Response." *Landslides* 16 (5): 1003–1020. <https://doi.org/10.1007/s10346-019-01159-x>.
- Ferretti, A., C. Prati, and F. Rocca. 2000. "Nonlinear Subsidence Rate Estimation Using Permanent Scatterers in Differential SAR Interferometry." *Geoscience and Remote Sensing, IEEE Transactions On* 38 (5): 2202–2212. <https://doi.org/10.1109/36.868878>.
- Fruneau, B., J. Achache, and C. Delacourt. 1996. "Observation and Modelling of the Saint-Étienne-de-Tinée Landslide Using SAR Interferometry." *Tectonophysics* 265 (3–4): 181–190. [https://doi.org/10.1016/S0040-1951\(96\)00047-9](https://doi.org/10.1016/S0040-1951(96)00047-9).
- Geudtner, D., R. Torres, P. Snoeij, M. Davidson, and B. Rommen. 2014. "Sentinel-1 System Capabilities and Applications." In *2014 IEEE Geoscience and Remote Sensing Symposium*, Quebec City, QC, Canada. 13–18 July 2014.
- Griggs, D. T., and N. E. Coles. 1954. *Creep of Single Crystals of Ice*. Vol. 11. Wilmette Ill: U.S. Army Snow Ice and Permafrost Research Establishment Corps of Engineers.
- Gupta, B. M., and C. R. Karisiddappa. 2000. "Modelling the Growth of Literature in the Area of Theoretical Population Genetics." *Scientometrics* 49 (2): 321–355. <https://doi.org/10.1023/a:1010577321082>.
- Herrera, G., R. Tomás, J. M. Lopez-Sanchez, J. Delgado, J. J. Mallorqui, S. Duque, and J. Mulas. 2007. "Advanced DInSar Analysis on Mining Areas: La Union Case Study (Murcia, SE Spain)." *Engineering Geology* 90 (3–4): 148–159.
- Highland, L. M., and P. Bobrowsky. 2008. *The landslide handbook—A guide to understanding landslides*, 129. Reston, Virginia: U.S. Geological Survey Circular. <https://pubs.usgs.gov/circ/1325/>.
- Hu, H., R. Tomás, X. Tang, J. López Vinielles, G. Herrera, T. Li, and Z. Liu. 2023. "Updating Active Deformation Inventory Maps in Mining Areas by Integrating InSar and LiDar Datasets." *Remote Sensing* 15 (4): 996.
- Iadanza, C., A. Trigila, P. Starace, A. Dragoni, T. Biondo, and M. Roccisano. 2021. "IdroGeo: A Collaborative Web Mapping Application Based on REST API Services and

- Open Data on Landslides and Floods in Italy.” *ISPRS International Journal of Geo-Information* 10 (2): 89.
- IGME. 1985a. *Mapa geotécnico y de riesgos geológicos para la ordenación urbana de Alcoy*. Mapa de riesgos geológicos E:1/25.000, 1/2.500 y 1/1.000. IGME.
- IGME. 1985b. *Mapa geotécnico y de riesgos geológicos para la ordenación urbana de Alcoy*. Mapa de Riesgos Geológicos E:1/25.000, 1/2500 y 1/1.000. Memoria. Madrid: Ministerio de Industria y Energía.
- Jia, H., Y. Wang, D. Ge, Y. Deng, and R. Wang. 2022. “InSAR Study of Landslides: Early Detection, Three-Dimensional, and Long-Term Surface Displacement Estimation—A Case of Xiaojiang River Basin, China.” *Remote Sensing* 14 (7): 1759.
- Knevels, R., H. Petschko, H. Proske, P. Leopold, D. Maraun, and A. Brenning. 2020. “Event-Based Landslide Modeling in the Styrian Basin, Austria: Accounting for Time-Varying Rainfall and Land Cover.” *Geosciences* 10 (6): 217.
- Koi, T., N. Hotta, I. Ishigaki, N. Matuzaki, Y. Uchiyama, and M. Suzuki. 2008. “Prolonged Impact of Earthquake-Induced Landslides on Sediment Yield in a Mountain Watershed: The Tanzawa Region, Japan.” *Geomorphology* 101 (4): 692–702. <https://doi.org/10.1016/j.geomorph.2008.03.007>.
- Kovács, I. P., T. Bugya, S. Czigány, M. Defilippi, D. Lóczy, P. Riccardi, L. Ronczyk, and P. Pasquali. 2019. “How to Avoid False Interpretations of Sentinel-1A TOPSAR Interferometric Data in Landslide Mapping? A Case Study: Recent Landslides in Transdanubia, Hungary.” *Natural Hazards* 96 (2): 693–712. <https://doi.org/10.1007/s11069-018-3564-9>.
- Lacroix, P. 2016. “Landslides Triggered by the Gorkha Earthquake in the Langtang Valley, Volumes and Initiation Processes.” *Earth Planets & Space* 68 (1): 46. <https://doi.org/10.1186/s40623-016-0423-3>.
- Li, Y., X. Fan, and G. Cheng. 2006. “Landslide and Rockfall Distribution by Reservoir of Stepped Hydropower Station in the Jinsha River.” *Wuhan University Journal of Natural Sciences* 11 (4): 801–805. <https://doi.org/10.1007/BF02830167>.
- Li, J., Z. W. Li, X. L. Ding, Q. J. Wang, J. J. Zhu, and C. C. Wang. 2014. “Investigating Mountain Glacier Motion with the Method of SAR Intensity-Tracking: Removal of Topographic Effects and Analysis of the Dynamic Patterns.” *Earth-Science Reviews* 138:179–195. <https://doi.org/10.1016/j.earscirev.2014.08.016>.
- Lin, W. T., W. C. Chou, C. Y. Lin, P. H. Huang, and J. S. Tsai. 2007. “Study of Landslides Caused by the 1999 Chi-Chi Earthquake, Taiwan, with Multitemporal SPOT Images.” *Canadian Journal of Remote Sensing* 33 (4): 289–302. <https://doi.org/10.5589/m07-036>.
- Liu, X., C. Zhao, Q. Zhang, Z. Lu, and Z. Li. 2020. “Deformation of the Baige Landslide, Tibet, China, Revealed Through the Integration of Cross-Platform ALOS/PALSAR-1 and ALOS/PALSAR-2 SAR Observations.” *Geophysical Research Letters* 47 (3): e2019GL086142. <https://doi.org/10.1029/2019GL086142>.
- Liu, X., C. Zhao, Q. Zhang, Y. Yin, Z. Lu, S. Samsonov, C. Yang, M. Wang, and R. Tomás. 2021. “Three-Dimensional and Long-Term Landslide Displacement Estimation by Fusing C- and L-Band SAR Observations: A Case Study in Gongjue County, Tibet, China.” *Remote Sensing of Environment* 267:112745. <https://doi.org/10.1016/j.rse.2021.112745>.
- Lomnitz, C. 1956. “Creep Measurements in Igneous Rocks.” *The Journal of Geology* 64 (5): 473–479. <https://doi.org/10.1086/626379>.
- Lomnitz, C. 1957. “Linear Dissipation in Solids.” *Journal of Applied Physics* 28 (2): 201–205. <https://doi.org/10.1063/1.1722707>.
- López-Vinielles, J., J. A. Fernández-Merodo, P. Ezquerro, J. C. García-Davalillo, R. Sarro, C. Reyes-Carmona, A. Barra, et al. 2021. “Combining Satellite InSAR, Slope Units and Finite Element Modeling for Stability Analysis in Mining Waste Disposal Areas.” *Remote Sensing* 13 (10): 2008.
- Lu, Z., and D. Dzurisin. 2010. “Ground Surface Deformation Patterns, Magma Supply, and Magma Storage at Okmok Volcano, Alaska, from InSAR Analysis: 2. Coeruptive Deflation, July–August 2008.” *Journal of Geophysical Research: Solid Earth* 115 (B5). <https://doi.org/10.1029/2009JB006970>.
- Luo, J., J. M. Lopez-Sanchez, F. De Zan, J. J. Mallorqui, and R. Tomás. 2022. “Assessment of the Contribution of Polarimetric Persistent Scatterer Interferometry on Sentinel-1 Data.” *IEEE Journal of Selected Topics in Applied Earth Observations & Remote Sensing* 15:7997–8009. <https://doi.org/10.1109/JSTARS.2022.3206550>.
- Massonnet, D., M. Rossi, C. Carmona, F. Adragna, G. Peltzer, K. Feigl, and T. Rabaute. 1993. “The Displacement Field of the Landers Earthquake Mapped by Radar Interferometry.” *Nature* 364 (6433): 138–142.
- Mondini, A. C., F. Guzzetti, K.-T. Chang, O. Monserrat, T. Ranjan Martha, and A. Manconi. 2021. “Landslide Failures Detection and Mapping Using Synthetic Aperture Radar: Past, Present and Future.” *Earth-Science Reviews* 216:103574. <https://doi.org/10.1016/j.earscirev.2021.103574>.
- Murray, K. D., R. B. Lohman, and D. P. S. Bekaert. 2021. “Cluster-Based Empirical Tropospheric Corrections Applied to InSAR Time Series Analysis.” *IEEE Transactions on Geoscience & Remote Sensing* 59 (3): 2204–2212. <https://doi.org/10.1109/TGRS.2020.3003271>.
- Navarro, J. A., M. Cuevas, A. Barra, and M. Crosetto. 2018. “Detection of Active Deformation Areas Based on Sentinel-1 Imagery: An Efficient, Fast and Flexible Implementation.” In *18th International Scientific and Technical Conference, Crete, Greece, 24–27 September 2018*.
- Navarro, J. A., M. Cuevas, R. Tomás, A. Barra, and M. Crosetto. 2019. “A Toolset to Detect and Classify Active Deformation Areas Using Interferometric SAR Data.” *Proceedings of the 5th International Conference on Geographical Information Systems Theory, Applications and Management, Heraklion, Crete, Greece, 3–5 May 2019*.
- Owen, L. A., U. Kamp, G. A. Khattak, E. L. Harp, D. K. Keefer, and M. A. Bauer. 2008. “Landslides Triggered by the 8 October 2005 Kashmir Earthquake.” *Geomorphology* 94 (1): 1–9. <https://doi.org/10.1016/j.geomorph.2007.04.007>.
- Rocscience. 2021. “Slide3. Documentation and Theory Overview.” Accessed 9 Oct, 2023. <https://www.rocscience.com/help/slide3/overview>.
- Skempton, A. W., and F. A. de Lory Stability of Natural Slopes in London Clay. In *Geotechnical Engineering for the Preservation of Monuments and Historical Sites, Proceedings of the 4th International Conference on Soil Mechanics and Foundation Engineering, 378–381. 12–24 August 1957*. Thomas Telford Publishing.
- Solari, L., M. Del Soldato, F. Raspini, A. Barra, S. Bianchini, P. Confuorto, N. Casagli, and M. Crosetto. 2020. “Review of Satellite Interferometry for Landslide Detection in Italy.” *Remote Sensing* 12 (8): 1351.

- Szeibert, W. T., R. Tomás, X. Liu, J. M. Lopez-Sanchez, E. Díaz, and C. Zhao. 2022. *Empleo de imágenes PAZ para la monitorización de un movimiento de ladera en Alcoy (Alicante) mediante interferometría SAR diferencial*. Granada, Spain: X Simposio Nacional sobre Taludes y Laderas Inestables.
- Tomás, R., E. Díaz, W. T. Szeibert, X. Liu, J. M. Lopez-Sanchez, and C. Zhao. 2023. “Geomorphological Characterization, Remote Sensing Monitoring, and Modeling of a Slow-Moving Landslide in Alcoy (Southern Spain).” *Landslides* 20 (6): 1293–1301. <https://doi.org/10.1007/s10346-023-02032-8>.
- Tomás, R., and Z. Li. 2017. “Earth Observations for Geohazards: Present and Future Challenges.” *Remote Sensing* 9 (3): 194. <https://doi.org/10.3390/rs9030194>.
- Tomás, R., J. I. Pagán, J. A. Navarro, M. Cano, J. L. Pastor, A. Riquelme, M. Cuevas-González, et al. 2019. “Semi-Automatic Identification and Pre-Screening of Geological–Geotechnical Deformational Processes Using Persistent Scatterer Interferometry Datasets.” *Remote Sensing* 11 (14): 1675.
- Torres, R., P. Snoeij, M. Davidson, D. Bibby, and S. Lokas. 2012. “The Sentinel-1 Mission and Its Application Capabilities.” In *2012 IEEE International Geoscience and Remote Sensing Symposium*, Munich, Germany, 22–27 July 2012.
- Torres, R., P. Snoeij, D. Geudtner, D. Bibby, M. Davidson, E. Attema, P. Potin, et al. 2012. “GMES Sentinel-1 Mission.” *Remote Sensing of Environment* 120:9–24. <https://doi.org/10.1016/j.rse.2011.05.028>.
- Tzouvaras, M., C. Danezis, and D. G. Hadjimitsis. 2020a. “Differential SAR Interferometry Using Sentinel-1 Imagery-Limitations in Monitoring Fast Moving Landslides: The Case Study of Cyprus.” *Geosciences* 10 (6): 236.
- Tzouvaras, M., C. Danezis, and D. G. Hadjimitsis. 2020b. “Small Scale Landslide Detection Using Sentinel-1 Interferometric SAR Coherence.” *Remote Sensing* 12 (10): 1560.
- USGS. 2022. “How Many Deaths Result from Landslides Each Year?” United States Geological Survey, Accessed December 18. <https://www.usgs.gov/faqs/how-many-deaths-result-landslides-each-year>.
- Wang, S. J., G. H. Li, Q. Zhang, and C. L. Lan. 2000. “Engineering Geological Study of the Active Tectonic Region for Hydropower Development on the Jinsha River, Upstream of the Yangtze River.” *Acta Geologica Sinica - English* 74 (2): 353–361.
- Wang, G., M. Xie, X. Chai, L. Wang, and C. Dong. 2013. “D-Insar-Based Landslide Location and Monitoring at Wudongde Hydropower Reservoir in China.” *Environmental Earth Sciences* 69 (8): 2763–2777. <https://doi.org/10.1007/s12665-012-2097-x>.
- Wasowski, J., and F. Bovenga. 2014. “Investigating Landslides and Unstable Slopes with Satellite Multi Temporal Interferometry: Current Issues and Future Perspectives.” *Engineering Geology* 174:103–138. <https://doi.org/10.1016/j.enggeo.2014.03.003>.
- Werner, C. L., U. Wegmüller, T. Strozzi, and A. Wiesmann. 2000. “Gamma SAR and Interferometric Processing Software.” *ERS - ENVISAT Symposium*, Gothenburg, Sweden, 16-20 Oct 2000.
- Xu, Y., J. Liu-Zeng, M. B. Allen, W. Zhang, and P. Du. 2021. “Landslides of the 1920 Haiyuan Earthquake, Northern China.” *Landslides* 18 (3): 935–953. <https://doi.org/10.1007/s10346-020-01512-5>.
- Xu, Q., Y. Yuan, Y. Zeng, and R. Hack. 2011. “Some New Pre-Warning Criteria for Creep Slope Failure.” *Science China Technological Sciences* 54 (1): 210–220. <https://doi.org/10.1007/s11431-011-4640-5>.
- Yao, J., X. Yao, and X. Liu. 2022. “Landslide Detection and Mapping Based on SBAS-Insar and PS-Insar: A Case Study in Gongjue County, Tibet, China.” *Remote Sensing* 14 (19): 4728.
- Yin, Y., X. Liu, C. Zhao, R. Tomás, Q. Zhang, Z. Lu, and B. Li. 2022. “Multi-Dimensional and Long-Term Time Series Monitoring and Early Warning of Landslide Hazard with Improved Cross-Platform SAR Offset Tracking Method.” *Science China Technological Sciences* 65 (8): 1891–1912. <https://doi.org/10.1007/s11431-021-2008-6>.
- Yin, Y., F. Wang, and P. Sun. 2009. “Landslide Hazards Triggered by the 2008 Wenchuan Earthquake, Sichuan, China.” *Landslides* 6 (2): 139–152. <https://doi.org/10.1007/s10346-009-0148-5>.
- Yunjun, Z., H. Fattahi, and F. Amelung. 2019. “Small Baseline InSar Time Series Analysis: Unwrapping Error Correction and Noise Reduction.” *Computers & Geosciences* 133:104331. <https://doi.org/10.1016/j.cageo.2019.104331>.
- Zhao, C., Y. Kang, Q. Zhang, Z. Lu, and B. Li. 2018. “Landslide Identification and Monitoring Along the Jinsha River Catchment (Wudongde Reservoir Area), China, Using the InSar Method.” *Remote Sensing* 10 (7): 993.
- Zhao, C., and Z. Lu. 2018. “Remote Sensing of Landslides—A Review.” *Remote Sensing* 10 (2): 279.